MAPPING OF THE BINDING SURFACE BETWEEN EPHA5 AND ANTAGONIST PEPTIDE BY NMR SPECTROSCOPY

ZHU WAN LONG

NATIONAL UNIVERSITY OF SINGAPORE

2009

MAPPING OF THE BINDING SURFACE BETWEEN EPHA5 AND ANTAGONIST PEPTIDE BY NMR SPECTROSCOPY

ZHU WAN LONG

A THESIS SUBMITTED FOR THE DEGREE OF

MASTER OF SCIENCE

DEPARTMENT OF BIOLOGICAL SCIENCES

NATIONAL UNIVERSITY OF SINGAPORE

2009

ACKNOWLEDGEMENTS

I would very much like to express my sincere appreciation to my supervisor, Associate Professor Song Jianxing for his support and experimental guidance thorough the duration of this study.

I would like to give my special thanks to Ms. Qin Haina for her help in determining the structure of WDC by NMR, and to Dr. Shi Jiahai for his work in determining the structure of EphA5 by X-ray crystallography.

I also want to thank Dr. Liu Jingxian, Ms. Huan Xuelu as well as all my lab mates for their valuable advices and help in this project. In addition, I am thankful to Dr. Fan Jingsong for all the NMR trainings and his kind assistance in NMR experiments.

Especially, I would like to thank my parents for their strong and continuous support and encouragement for my study.

Finally, I am grateful to the Ministry of Education of Singapore for the scholarship support and National University of Singapore for the excellent post-graduate programme and research environment.

Table of Contents

SUMMARY

The Eph receptors constitute the largest family of receptor tyrosine kinases, with 16 individual receptors that are activated by 9 different ephrins throughout the animal kingdom. Eph receptors and their ligands are both anchored to the plasma membrane, and are subdivided into two subclasses (A and B) based on their sequence conservation and binding preferences. The critical roles of Eph-ephrin mediated signalling in various physiological and pathological processes mean that the interface at which the interaction between receptor and ligand occurs is a promising target for the development of molecules to treat human diseases, such as neuron regeneration, bone remodelling diseases, and cancer.

A diverse spectrum of peptides that act as antagonists of Eph-ephrin with differential selectivity has previously been identified. One of these peptides, called WDC, is attractive because it has been found to antagonize the interaction between EphA5 and its ligands with high selectivity. EphA5 receptor and its ligands serve as repulsive axonguidance cues in the developing brain. Their interaction triggers growth cone collapse and inhibits the neurite outgrowth in vitro. Furthermore, abnormal expression of these molecules would result in the disruption of axonal path finding and mid-line crossing in vivo. So far, the three-dimensional structure of the EphA5 ligand-binding domain has not been determined.

In the present study, the crystal of EphA5 ligand-binding domain was obtained. Structural characterizations of both EphA5 and WDC were assessed by CD and NMR.

Furthermore, characterizations of binding interactions between EphA5 and WDC peptide were characterized by NMR and ITC. The binding surface between EphA5 and WDC was demonstrated using NMR.

Interestingly, WDC was found to be well-folded even in the free-state. Its binding surface for EphA5 receptor was mapped by Ala site-directed mutagenesis and NMR titration. Taken all together, our results may provide critical rationales for further design of specific EphA5 antagonists for various therapeutic applications.

LIST OF FIGURES

LIST OF TABLES

LIST OF ABBREVIATIONS

1D/2D/3D	One-/Two-/Three-dimensional
a.a.	Amino acid
cDNA	Complementary DNA
CD	Circular Dichroism
CS	Chemical Shift
Da (kDa)	Dalton (kilodalton)
DNA	Deoxyribonucleic Acid
DTT	Dithiothreitol
E. coli	*Escherichia coli*
EDTA	Ethylenediaminetetraacetic Acid
Eph	Erythropoietin Producing Hepatocellular Receptor
FID	Free Induction Decay
FPLC	Fast Protein Liquid Chromatography
g/mg/µg	Gram/Milligram/Microgram
GndHCl	Guanidine Hydrochloride
GST	Gluthathione S-transferase
HSQC	Heteronuclear Single Quantum Coherence
IPTG	Isopropyl-β-D-thiogalactopyranoside
l/ml/µl	Liter/Milliter/Microliter
LB	Luria Bertani

MALDI-TOF MS	Matrix-Assisted Laser Desorption/Ionization Time-of-flight Mass Spectroscopy
min	Minute
M (mM)	Mole/L (Milimole/L)
MR	Molecular Replacement
MW	Molecular Weight
NMR	Nuclear Magnetic Resonance
NOE	Nuclear Overhauser Effect
NOESY	Nuclear Overhauser Effect Spectroscopy
OD	Optical Density
PBS	Phosphate-buffered Saline
PCR	Polymerase Chain Reaction
PDB	Protein Data Bank
ppm	Parts Per Million
RMSD	Root Mean Square Deviation
RP-HPLC	Reversed-Phase High Performance Liquid Chromatography
SDS-PAGE	Sodium Dodecyl Sulfate Polyacrylamide Gel Eletrophoresis
TOCSY	Total Correlation Spectroscopy
Tris	2-amino-2-hydroxymethyl-1,3-propanediol
UV	Ultraviolet
βME	β-Mercaptoethanol

APPENDIX

Chapter I INTRODUCTION

1.1 Introduction to Eph Receptors

1.1.1 Biological background of Eph receptors

The erythropoietin-producing hepatocellular carcinoma (Eph) family is the largest family of receptor tyrosine kinases identified to date, with 16 structurally similar family members (Eph Nomenclature Committee, 1997). Eph is divided into two subclasses, A and B, based on binding preferences and sequence conservation. In general, EphA receptors (EphA1–EphA10) bind to glycosyl phosphatidyl inositol (GPI)-anchored ephrinA ligands (ephrinA1–ephrinA6), whereas EphB receptors (EphB1–EphB6) interact with transmembrane ephrinB ligands (ephrinB1–ephrinB3). Although the interactions between Eph receptors and eprhins in the same subclass are quite promiscuous, the interactions between subclasses are relatively rare (Pasquale, 2008; Gale *et al.* 1996; Qin *et al.* 2008).

As shown in Figure 1, Eph receptors have a modular structure that consists of an N-terminal ephrin binding domain adjacent to a cysteine-rich domain and two fibronectin type III repeats in the extracellular region. The intracellular region consists of a juxtamembrane domain, a conserved tyrosine kinase domain, a C-terminal sterile a-domain, and a PDZ binding motif. The N-terminal 180 amino acid globular domain is sufficient for high-affinity ligand binding. The adjacent cysteine-rich region might be involved in receptor–receptor oligomerization often observed on ligand binding (Qin *et al.* 2008; Pasquale 2005).

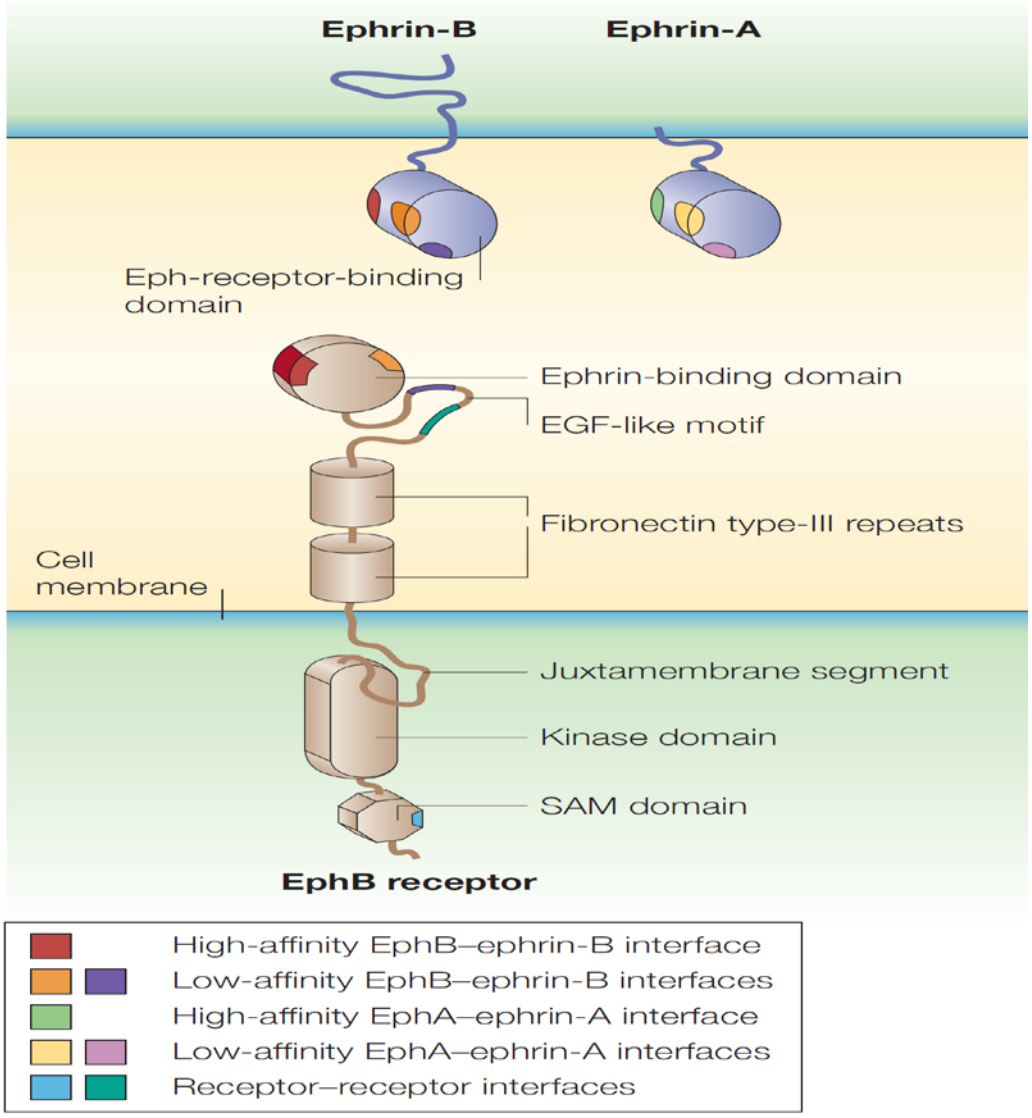

Figure 1: Domain structure and binding interfaces of Eph receptors and ephrins. (Pasquale, 2005)

The communication of biochemical signals between cells is essential for the development and existence of multicellular organisms. The direct protein-protein interactions between ligands carrying the signal, and cell-surface receptors recognizing and transforming the information into the receiving cell are the key method of communication (Himanen *et al.* 2001). Being one of the large groups of receptors and ligands, the Eph/ephrin family sends information bidirectionally into both the receptor-expressing cell and the ligand-expressing cell (Pasquale 2005; Flanagan *et al.* 1998; Himanen *et al.* 2003; Kullander *et al.* 2002). Upon ephrin binding, the tyrosine kinase domain of the Eph receptors is activated and therefore, initiating 'forward' signalling in the receptor-expressing cells. At the same time, signals are also induced in the ligand-expressing cells, a phenomenon referred to as 'reverse' signalling (Holland *et al.* 1996; Himanen *et al.* 2007).

The Eph/ephrin family plays important roles in both developing and adult tissues, and regulates biological processes such as tissue patterning, development of the vascular system, axonal guidance, and neuronal development (Pasquale, 2005; Pasquale, 2008; Brantley-Sieders *et al.* 2004). It also has been shown to function in bone remodelling, immunity, blood clotting, and stem cells. Recently, the Eph-ephrinB-mediated signalling network has been implicated in learning and memory formation, neuronal regeneration, pain processing, and differential expressions of ephrinB are also correlated with tumorigenesis (Battaglia *et al.* 2003; Ran *et al.* 2005).

1.1.2 Structures of Eph receptors and Eph receptor/ephrin complexes

Because the Eph receptors/ephrins play very important roles in various biological

progresses, the structural study of these Eph/ephrins will help us to understand the detailed mechanism of the binding and recognition between Eph receptors and ephrin ligands. The structures of the ligand-binding domains of EphA2, EphA4, EphB2 and EphB4 have been determined in the Free State and in complex with ephrins or peptide antagonists by X-ray crystallography (Qin *et al.* 2008; Himanen *et al.* 2001; Himanen *et al.* 2004; Chrencik *et al.* 2006; Chrencik *et al.* 2006; Chrencik *et al.* 2007; Himanen *et al.* 2009). These studies have shown that all the Eph ligand-binding domains adopt the same jellyroll β-sandwich architecture that are composed of 11 antiparallel β-strands connected by loops of various lengths, although they belong to different subclass of Eph receptors (Figure 2). Although the H-I loop has no regular secondary structure in all the examined EphB receptor structures, the EphA2 and EphA4 receptors form a 3_{10}-helix in the H-I loop.

The crystal structures of Eph ligand-binding domains and ephrin indicate that initial high affinity binding of Eph receptors to ephrin occurs through the penetration of an extended G–H loop of the ligand into a hydrophobic channel on the surface of the receptor. In particular, the D-E and J-K loops have been revealed to play a critical role by forming the high affinity Eph-ephrin binding channel (Himanen *et al.* 2009).

The structure of the EphB2-ephrinB4 complex showed that the ligand-binding channel of the receptor is located at the upper convex surface of EphB2, and is formed by the flexible J-K, G-H, and D-E loops, which become ordered to accommodate the solvent-exposed ephrin G-H loop (Figure 3). A low affinity tetramerization interface, which interacts with the C-D loop of the ephrin has also been identified at the concave surface of the receptor H-I loop (Chrencik *et al.* 2006).

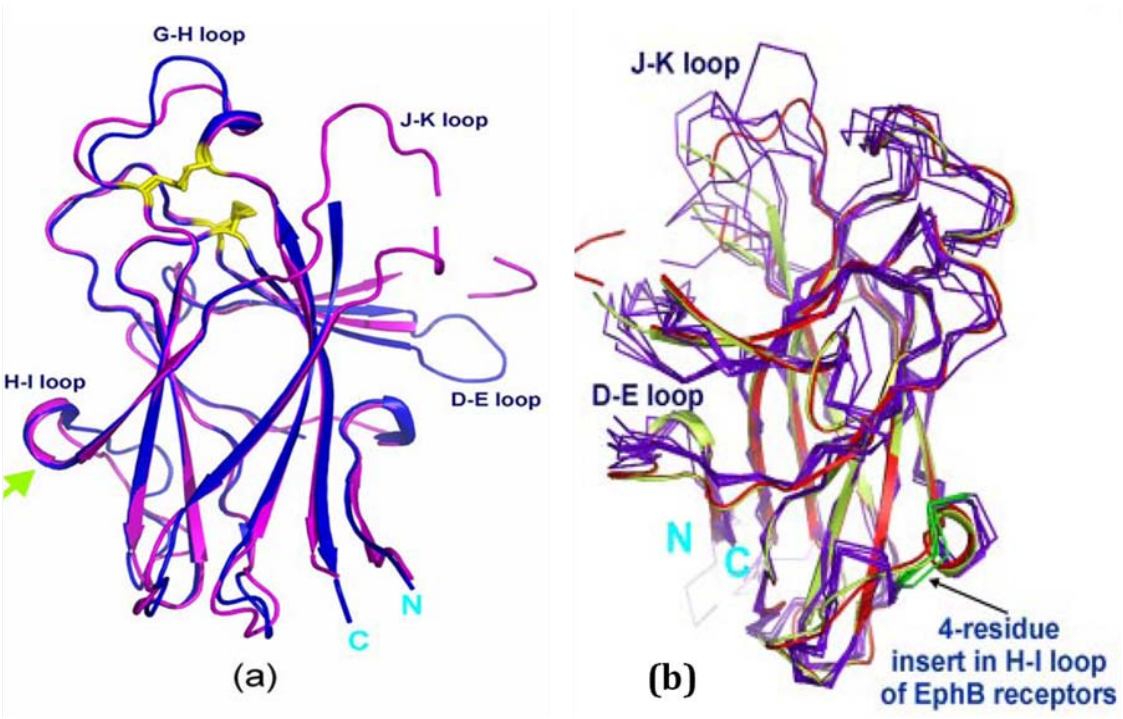

Figure 2: Structural comparisons of EphA4 and other Eph ligand-binding domains. (a) Superimposition of the ligand-binding domains of EphA4 Structure A (violet) and EphA2 (3C8X; blue). (b) Stereo view of the superimposition of two EphA4 structures (structure A in red and structure B in lime green) with previously determined EphB2 and EphB4 structures (all in purple). (Qin *et al*. 2008)

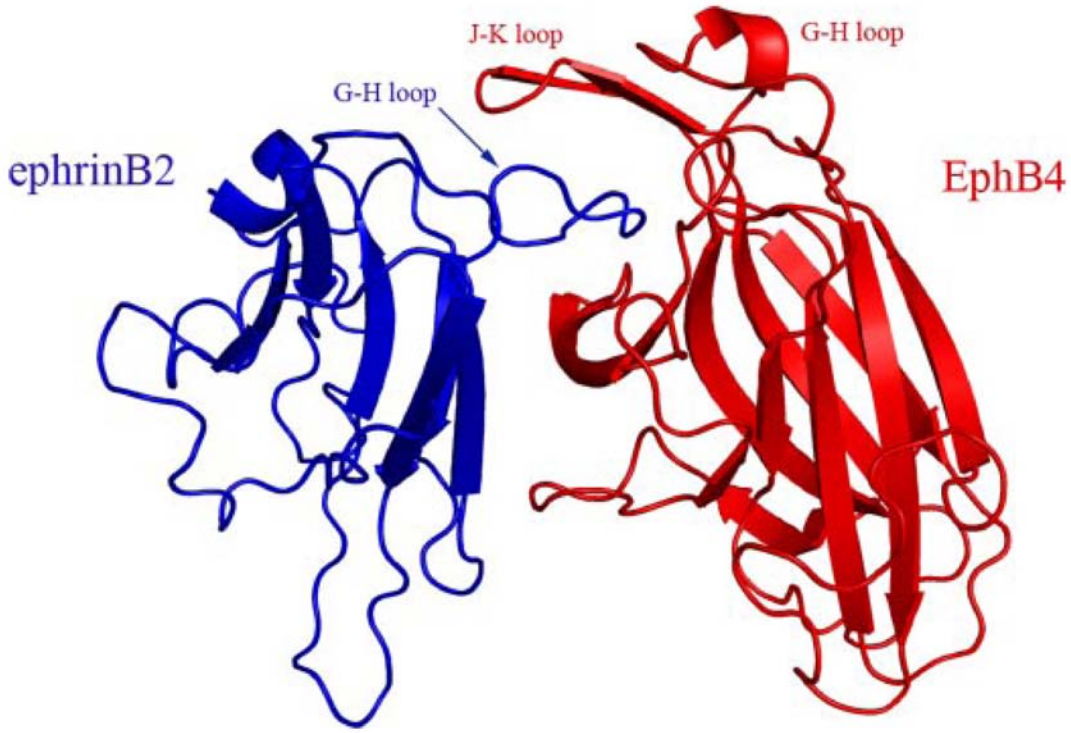

Figure 3: Ephrin binding domain of EphB4 receptor in complex with the ephrinB2 extracellular domain. EphB4 receptor (red) consists of a jellyroll folding topology with 13 anti-parallel B-sheets connected by loops of varying lengths, whereas the ephrin ligand (blue) is similar to the Greek key folding topology. The interface is formed by insertion of the ligand G-H loop into the hydrophobic binding cleft of EphB4. (Chrencik *et al.* 2006)

The EphA2/ephrinA1 heterodimer is architecturally similar to the EphB2-ephrinB4 complexes (Figure 3). The ligand/receptor interface centers around the G–H loop of ephrinA1, which is inserted in a channel on the surface of EphA2 (Figures 4). Eph receptor strands D, E and J, define the two sides of the channel, whereas strands G and M line its back. The ligand binds by approximating the side of its β-sandwich to the outside surface of the channel and then inserting its long G–H loop into the channel, which finally becomes buttressed by the G–H loop of the receptor closing in from the top. The binding is dominated by the Van der Waals contact between two predominantly hydrophobic surfaces. Adjacent to the channel/G–H-loop interactions, a second, structurally separate, contact area encompasses the ephrinA1 docking site along the upper surface of the receptor. Here, the ephrin β-sandwich (strands C, G and F) interacts through a network of hydrogen bonds and salt bridges with EphA2 strands D, E and the B–C loop region (Himanen *et al.* 2009).

Comparison of the EphA2/ephrinA1 structure with the EphB2/ephrinB4 complexes yields insight into the molecular basis for the observed Eph receptor/ephrin subclass specificity (Figures 3, 4). Eph receptor subclass specificity is probably maintained in part by the fact that the differences in the structures of the A- and B-class molecules result in different architectural arrangements of ligands and receptors in the A- and B-subclass complexes. Figures 3 and 4 illustrate that the B-class complexes adopt a more ‘compact’ conformation with intimate interactions between the Eph receptor B–C region and the juxtaposing C, F and G ephrin strands, whereas the A-class complex is more ‘open’ with a smaller number of interactions in the above-mentioned region, but with a more intimate interaction network between the ephrin G-H loop and the D–E, J–K

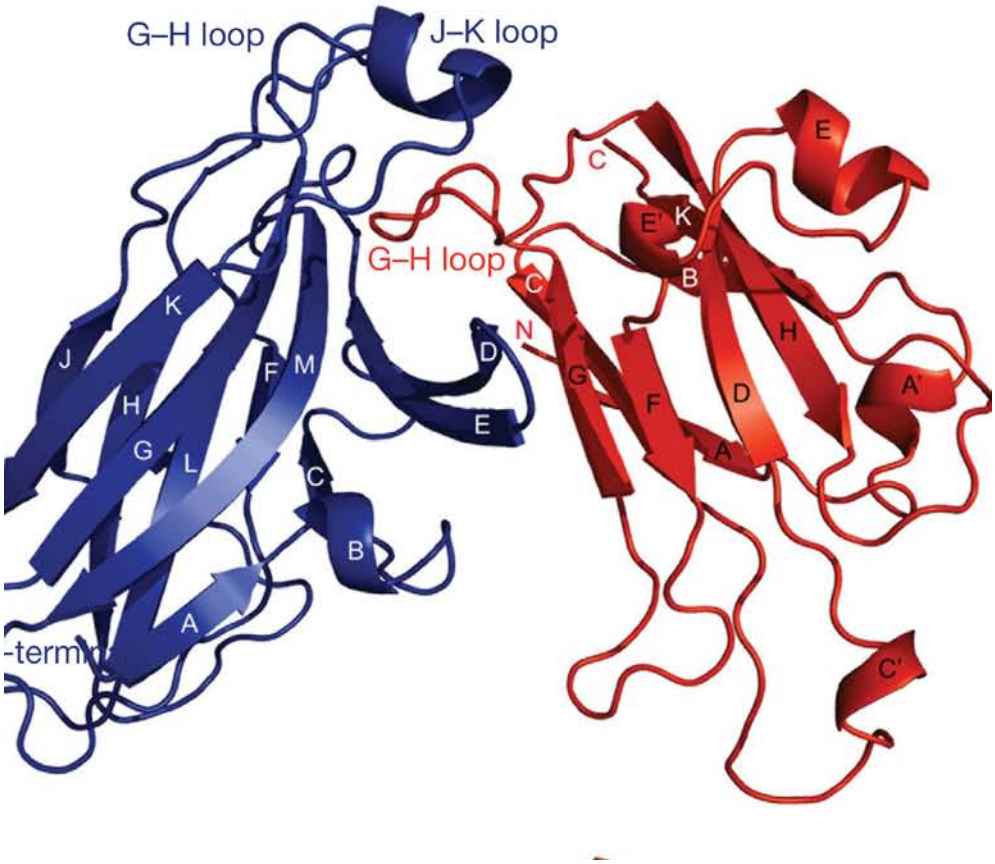

Figure 4: Ephrin binding domain of the EphA2 receptor in complex with the ephrinA1 extracellular domain EphA2. EphA2 (Blue): residues Glu28–Cys201 and ephrin-A1 (Red): residues Ala18–Ile151. (Himanen *et al.* 2009)

and G–H loops of Eph receptor (Himanen *et al.* 2009).

The different complex structures suggest that the interactions between receptor and ligand in the A-class Eph receptor/ephrin involve smaller rearrangements in the interacting partners, better described by a ’lock-and-key’-type binding mechanism, in contrast to the ’induced fit’ mechanism defining the B-class molecules (Himanen *et al.* 2009).

1.1.3 Drug designs from the structural insights of Eph receptors and ephrin ligands

As the Eph receptors constitute the largest RTK family, imbalance of Eph/ephrin function may therefore contribute to a variety of diseases, such as diabetes, tumor, spinal cord injury, abnormal blood clotting and bone remodeling diseases. The critical roles of Eph receptors in various physiological and pathological processes have validated the Eph receptor as the promising targets for the development of anti-tumor and neuronal regeneration drugs (Tang *et al.* 2007; Fry *et al.* 2005; Klein 2004; Yamaguchi *et al.* 2004; Goldshmit *et al.* 2004; Fabes *et al.* 2006; Fabes *et al.* 2007).

According to the structural information for Eph receptors and ephrin ligands, the majority of the Eph receptor/ephrin interactions involve the extended G–H ephrin loop interacting with the Eph receptor surface channel. It has been proposed that some small peptides and chemical compounds could bind to the Eph receptor channel and block Eph receptor signaling by preventing ephrin binding to Eph receptor (Qin *et al.* 2008; Koolpe *et al.* 2002; Chrencik *et al.* 2006; Chrencik *et al.* 2007; Koolpe *et al.* 2002).

Despite the presence of several binding interfaces, peptides that target the high affinity site are sufficient to inhibit Eph receptor-ephrin binding. Interestingly, unlike the

ephrins, which bind in a highly promiscuous manner, a number of the peptides that were identified by phage display selectively bind to only one or a few of the Eph receptors (Koolpe *et al.* 2005; Chrencik *et al.* 2007). The antibodies and soluble forms of Eph receptors and ephrins extracellular domains that modulate Eph-ephrin interactions have also been identified (Pasquale, 2005; Ireton *et al.* 2005; Noren *et al.* 2007; Wimmer-Kleikamp *et al.* 2005). Several small inhibitors of the Eph receptor kinase domain have also been reported. These inhibitors occupy the ATP-binding pocket of the receptors and are usually broad specificity inhibitors that target different families of tyrosine kinases (Caligiuri *et al.* 2006; Karaman *et al.* 2008).

Recently, two small molecules (2,5-dimethylpyrrolyl benzoic acid derivative and its isomeric compound) have been identified by a high throughput screening, which are able to antagonize ephrin-induced effects in EphA4-expressing cells. The antagonizing benzoic acid derivatives occupy a cavity in the ephrin-binding EphA channel by interacting with residues Ile^{31}–Met^{32} in the D–E loop, Gln^{43} in the E strand, and Ile^{131}–Gly^{132} in the J–K loop (Noberini *et al.* 2008; Qin *et al.* 2008).

1.1.4 Functions of EphA5 receptor

EphA5 receptor is a member of the Eph receptor tyrosine kinase family. It is thought to be wildly expressed in most tissues, and higher expression mainly occurs in the hippocampus, striatum, hypothalamus, and amygdale in the adult brain (Gerlai *et al.* 1999).

The function of the EphA5 receptor is best characterized as an axon guidance molecule during neural development. EphA5 receptor and its ligands act as a repellent

cue that prevents axons from entering inappropriate territories, thus restricting the cells to specific pathways during the migratory process. During neural development, Eph receptors and their ligands are expressed in the projecting and target sites, respectively (Wilkinson, 2001; Castellani *et al.* 1998).

At the cellular level, the binding of EphA5 receptors with ligands expressing neurons results in different consequences depending on the cell type. It has been demonstrated that this interaction causes inhibition of the neurite outgrowth of the hippocampal, striatal, retinal, and cortical neurons (Brownlee *et al.* 2000). At the circuit level, over expression of a truncated form of EphA5 receptor results in a miswiring of the hippocamposeptal pathway and corpus callosum connections in vivo (Yue *et al.* 2002).

Taken together, EphA5 receptor and its ligands serve as repulsive axonguidance cues in the developing brain. Their interaction triggers growth cone collapse and inhibits the neurite outgrowth in vitro. Furthermore, abnormal expression of these molecules results in the disruption of axonal path finding and mid-line crossing in vivo (Hu *et al.* 2003).

1.2 Structure Determination of Protein/peptide

Proteins are organic compounds made of amino acids arranged in a linear chain. Proteins are an important class of biological macromolecules and present in all living organisms. The function of a protein at the molecular level can be better understood by determining its three dimensional structure. Common experimental methods of structure determination include X-ray crystallography, NMR spectroscopy, and cyro-electron microscopy. Both X-ray crystallography and NMR spectroscopy can yield information at

atomic resolution.

1.2.1 Introduction to NMR spectroscopy

1.2.1.1 NMR

Nuclear magnetic resonance (NMR) is a property that magnetic nuclei have when they are placed in a magnetic field and apply electromagnetic (EM) pulse, which cause the nuclei to absorb energy from the EM pulse and then radiate it back out. The NMR phenomenon was first detected by Bloch and Purcell independently in 1946 (Bloch, 1946; Purcell, 1946), for which they shared the Noble Prize in 1952. NMR spectroscopy was first used in the structural determination of small molecules in organic chemistry. The application of NMR to protein structure determination only started after Wuthrich developed the 2D experiment in the early 1980s (Wuthrich, 1986).

Nowadays, NMR has become as powerful a technique as X-ray crystallography for determining the three dimensional structures of biological macromolecules. So far, NMR is the only method for solving protein structure in solution. Furthermore, NMR is also available for studying protein dynamics, protein folding and protein/protein interaction. With the improved NMR hardware, better developed NMR methodology and advanced computer, and multidimensional NMR spectroscopic techniques, today NMR has been widely applied in the areas of chemistry, biology and medicine.

1.2.1.2 NMR parameters

1.2.1.2.1 Chemical shift

Chemical shift, which is caused by electric de-shielding effect, is an important parameter for identifying individual nucleus and assigning the resonances in the spectrum to their corresponding atoms in a molecule. The nuclei within different chemical environment will have different resonance frequencies and appear in the spectrum at different positions. The reason is that electrons circulating about the direction of the applied external magnetic field and the circulation will then cause the generation of a small magnetic field at the nucleus. Therefore, each nucleus in an NMR spectrum gives rise to a resonance which is characterized by chemical shift that reflects its unique chemical environment.

The characteristic chemical shifts in the amino acids will be helpful for identifying individual residues in a protein and determining the protein secondary structure by comparing the observed chemical shifts with random coil values (Wishart *et al.* 1991). In order to measure the chemical shift independent of the static magnetic field strength, parts per million (ppm) is used to present chemical shift of nucleus.

1.2.1.2.2 J coupling

J coupling is also referred to as spin-spin coupling or scalar coupling, which is mediated through chemical bonds between two spins. Scalar couplings are used in multidimensional (2D, 3D, 4D) correlation experiments to transfer magnetization from one spin to another in order to identify spin systems. Normally, couplings over one bond, two bonds and three bonds are observed (Sattler, 2004). There are two types of J couplings: homonuclear and heteronuclear coupling. In homonuclear coupling, the coupled nuclei have the same magnetogyric ratio γ, but different chemical shift, such as

proton-proton coupling. In heteronuclear coupling, the coupled nuclei have different magnetogyric ratio γ, such as coupling between nuclei ^{1}H-^{15}N, ^{1}H-^{13}C, or ^{15}N-^{13}C.

1.2.1.2.3 NOE

NOE (nuclear Overhauser effect) is a dipolar cross-relaxation phenomenon between spins through space magnetization transfer. As a function of interproton distances NOE is proportional to the inverse sixth power of the distance (NOE ~ $1/r^6$) between protons at short mixing time. If the interproton distances are larger than 5 Å, the NOE probably is too small to be observed.

NOE provides much information for the 3D structure determination of protein. Intra-residue and sequential NOEs not only provide information for establishing connections among amino acids, but also reveal protein secondary structure through the observed NOE patterns. More importantly, long-range NOE interactions, which can correlate protons far apart from protein sequence but close together in space, provide the principle source of information for the determination of protein tertiary structure in NMR (Wüthrich, 1986).

1.2.2 Introduction to X-ray crystallography

1.2.2.1 X-ray crystallography

X-ray crystallography is a method of determining the arrangement of atoms within a crystal, in which a beam of X-rays strikes a crystal and diffracts into many specific directions. A three-dimensional picture of the density of electrons within the crystal can be produced from the angles and intensities of these diffracted beams. And the mean

positions of the atoms, their chemical bonds, and disorder in the crystal can then be determined by the electron density data.

X-ray was firstly discovered by the German physicist, Wilhelm Conrad Röntgen in 1895. In 1912-1913, William Lawrence Bragg developed Bragg's law, which connects the observed scattering with reflections from evenly spaced planes within the crystal. In 1915, He and his father (William Henry Bragg) shared the Noble Prize in Physics.

The first crystal structures of protein, sperm whale myoglobin, was solved by Max Perutz and Sir John Cowdery Kendrew, for which they were awarded the Nobel Prize in Chemistry in 1962 (Kendrew, 1956). So far, over 48970 X-ray crystal structures of proteins, nucleic acids and other biological molecules have been determined. Crystallography has a big advantage on solving structures of arbitrarily large molecules, whereas solution-state NMR is restricted to relatively small ones (less than 70 kDa).

1.2.2.2 Solution to phase problem

Direct methods, isomorphous replacement method, anomalous scattering method and molecular replacement are the four methods used to solve the phase problem in macromolecular structure determination. All these methods only yield phase estimates for a limited set of reflections. To improve the accuracy of the phase and to get an interpretable electron density map, refinement at both reciprocal and real space is carried out with the help of Fourier transformation.

1.2.2.2.1 Direct methods

The direct method relies on the possible development of useful statistical

relationships between sets of structure factors to deduce their phases. However, a crystal to be made up of similarly-shaped atoms with positive electron density everywhere must be assumed. The direct methods estimate the initial phases for a selected set of reflections using a triple relation and extend phases to more reflections. A triple relation is one where there are trio of reflections in which the intensity and phase of one reflection can be explained by the other two. High resolution data (> 1.2 Å) will be required for the direct methods to be successfully applied in protein crystallography (Hauptman H, 1997). Therefore, this method is limited to the structure determination of small molecules.

1.2.2.2.2 Multiple isomorphous replacement (MIR)

Multiple isomorphous replacement is the most common approach of solving the phase problem in X-ray crystallography. This method is conducted by soaking the crystal of a sample to be analyzed in a heavy atom solution or by co-crystallization the sample with the heavy atom. X-ray data sets from the native crystal soaked in a specific heavy atom, such as mercury, platinum or gold are collected. For the determination of derivative and the positions of the heavy atoms, another data set is then collected by using difference Patterson maps. Once the initial heavy atom locations have been determined, the coordinates, occupancy and temperature factors of each heavy atom are refined. For the structure determination by MIR, at least two isomorphous derivatives must be evaluated since using only one will give two possible phases (Taylor, 2003).

1.2.2.2.3 Anomalous scattering

In X-ray crystallography, anomalous scattering refers to a change in a diffracting

X-ray's phase that is unique from the rest of the atoms in a crystal due to strong X-ray absorbance. Two techniques which are based on anomalous scattering used in X-ray crystallography are multi-wavelength anomalous dispersion (MAD) and single-wavelength anomalous dispersion (SAD). In MAD, the most commonly used atom for phase determination is selenium (Ealick, 2000). The selenium is introduced into the crystal to replace the natural sulfur containing amino acid methionine by selenomethionine, and at least two sets of data are collected at different wavelength. However, SAD only uses a single dataset at a single appropriate wavelength. The advantage of SAD in contrast to MAD is the minimization of time spent in the beam by the crystal, thus reducing potential radiation damage to the molecule while collecting data.

1.2.2.2.4 Molecular replacement (MR)

The molecular replacement method is used to solve the phase problem when the protein molecule has high sequence and structural similarity to an already solved protein structure. Firstly, a patterson map, which is considered as a fingerprint of a protein structure, is computed from an already solved homologous protein structure. Secondly, the patterson map of the homology model is then correctly orientated in the new crystal unit-cell by means of rotation functions. Finally, the best fit is achieved by translation through the support of a convincing correlation factor and a residual factor.

1.2.2.3 Refinement of initial model

Because the built initial model is usually not optimal, refinement is needed to improve the model. Refinement of a model is the optimization of a function of a set of

observations so that the correlation between the atomic model and the diffraction data is maximized. Two R factors (*R*-factor and R_{free}-factor) which reflect the quality of the data are monitored during the refinement. *R*-factor (also refers to 'reliability') is the agreement index between the refined structural models and experimentally observed X-ray diffraction data. R_{free}-factor is the factor calculated from a subset (~10%) of reflections that were not included in the structure refinement.

1.3 Research Aims

EphA5 receptor plays a very important role in the growth of neuron and many signal pathways as mentioned above. However, the three dimensional structure of EphA5 ligand-binding domain has so far not been determined by NMR or X-ray crystallography. Furthermore, Prof. Elena Pasquale and many other scientists have designed some peptide inhibitors that inhibit the binding of EphA5 receptor with its ligands.

The research aim of this study has focused on three points.

(1) To crystallize the EphA5 ligand-binding domain and to resolve its three dimensional structure by X-ray crystallography.

(2) To determine the binding affinity of EphA5 receptor with its antagonistic peptides by different biophysical and biochemical methods.

(3) To map the binding surface between WDC and EphA5 receptor by NMR spectroscopy.

Chapter II MATERIALS AND METHODS

2.1 Cloning of Proteins and/or Peptides

The DNA fragment encoding for the human EphA5 ligand-binding domain (residues 59–235) was amplified from a HeLa cell cDNA library using two primers containing *Bam*HI and *Xho*I restriction sites, 5'-GGA TCC AAC GAA GTG AAT TTA TTG GAT TCA CGC -3' (forward) and 5'-CTC GAG TCA AGA AGG CGC TTC TTT ATA GTA TAC -3'(reverse). The PCR fragment was cloned into a *Bam*HI and *Xho*I cut pET32a vector (Novagen), and the resulting construct was transformed into *Escherichia coli* Rosetta-gami (DE3) cells (Novagen), allowing more efficient formation of disulfide bonds and expression of eukaryotic proteins containing codons rarely used by *E. coli*. The free Cys^{233} in this construct was mutated to Ala by use of the site-directed mutagenesis kit (Stratagene) to avoid the formation of non-native disulfide bridges.

PCR-based strategy was utilized to synthesize the genes encoding WDC peptide (peptide sequence: WDCNGPYCHWLG) (Wei *et al.* 2005). Briefly, the gene encoding WDC was obtained by PCR with two long oligonucleotides: Forward Primer (5'-GGA TCC TGG GAT TGC AAC GGC CCG TAT TGC CAT TG -3') and Reverse Primer (5'-CTC GAG TCA GCC CAG CCA ATG GCA ATA CGG GCC-3') with a 17-mer overlap designed with *E. coli* preferred codons containing *Bam*HI and *Xho*I restriction sites. The PCR fragment was cloned into a *Bam*HI and *Xho*I cut pGEX-4T-1 vector (Amersham Biosciences), and the vector was transformed into *E. coli* Rosetta-gami (DE3) cells (Novagen), as described above.

2.2 Selection of Residues for Sit-directed Mutagenesis

In order to identify the residues in WDC that bind with EphA5, an alanine site-directed mutagenesis screen of WDC was conducted. PCR-based strategy was also utilized to synthesize the genes encoding WDC-mutant peptides as described above. The mutated peptide sequences and the DNA oligo nucleotides are listed in Table 1. The PCR fragment was cloned into a *Bam*HI and *Xho*I cut pGEX-4T-1 vector (Amersham Biosciences), and the resulting construct was transformed into *E. coli* Rosetta-gami (DE3) cells (Novagen), as described above. All DNA constructs were confirmed by automated sequencing prior to expression of the recombinant proteins.

2.3 Transformation of *E. coli* Cells

Two microliters of plasmid DNA was transferred to the tube containing 50 µL of *E. coli* competent cells and gently mixed. The cells were then cooled on ice for 30 min, followed by a heat shock at 42°C for 90 seconds and then cooled on ice for 2 min. LB medium (500 µL) was added to the tube and incubated for 1 hr at 37°C with shaking at 100 rpm. After incubation, the cells were plated onto LB Agar plates containing 100 µg/ml ampicillin.

2.4 Expression and Purification of EphA5 and Peptides

2.4.1 Expression and purification of the EphA5 ligand-binding domain

Table 1: Mutants of WDC peptide and their corresponding oligo nucleotides

Name	Amino Acid sequence	Primers	
1WA	***A***DCNGPYCHWLG	Forward	5'-GGA TCC ***GCG*** GAT TGC AAC GGC CCG TAT TGC CAT TG-3'
		Reverse	5'-CTC GAG TCA GCC CAG CCA ATG GCA ATA CGG GCC-3'
2DA	W***A***CNGPYCHWLG	Forward	5'-GGA TCC TGG ***GCG*** TGC AAC GGC CCG TAT TGC CAT TG-3'
		Reverse	5'-CTC GAG TCA GCC CAG CCA ATG GCA ATA CGG GCC-3'
4NA	WDC***A***GPYCHWLG	Forward	5'-GGA TCC TGG GAT TGC ***GCG*** GGC CCG TAT TGC CAT TG-3'
		Reverse	5'-CTC GAG TCA GCC CAG CCA ATG GCA ATA CGG GCC-3'
6PA	WDCNG***A***YCHWLG	Forward	5'-GGA TCC TGG GAT TGC AAC GGC ***GCG*** TAT TGC CAT TG-3'
		Reverse	5'-CTC GAG TCA GCC CAG CCA ATG GCA ATA ***CGC*** GCC-3'
7YA	WDCNGP***A***CHWLG	Forward	5'-GGA TCC TGG GAT TGC AAC GGC CCG ***GCG*** TGC CAT TG-3'
		Reverse	5'-CTC GAG TCA GCC CAG CCA ATG GCA ***CGC*** CGG GCC-3'
9HA	WDCNGPYC***A***WLG	Forward	5'-GGA TCC TGG GAT TGC AAC GGC CCG TAT TGC ***GCG***TG-3'
		Reverse	5'-CTC GAG TCA GCC CAG CCA ***CGC*** GCA ATA CGG GCC-3'
10WA	WDCNGPYCH***A***LG	Forward	5'-GGA TCC TGG GAT TGC AAC GGC CCG TAT TGC CAT ***GC***-3'
		Reverse	5'-CTC GAG TCA GCC CAG ***CGC*** ATG GCA ATA CGG GCC-3'
11LA	WDCNGPYCHW***A***G	Forward	5'-GGA TCC TGG GAT TGC AAC GGC CCG TAT TGC CAT TG-3'
		Reverse	5'-CTC GAG TCA GCC ***CGC*** CCA ATG GCA ATA CGG GCC-3'

The recombinant EphA5 was over expressed in *E. coli* Rosetta-gami (DE3) cells. Briefly, the cells were cultured in Luria-Bertani medium at 37°C until the absorbance at 600 nm reached ~0.6. Isopropyl 1-thio-D-galactopyranoside (IPTG) was then added to a final concentration of 0.1 mM to induce EphA5 expression at 18°C for overnight. The harvested cells were sonicated in the lysis buffer containing 20 mM sodium phosphate (pH 7.3) and 150 mM sodium chloride to release soluble His-tagged proteins, which were subsequently purified by affinity chromatography using nickel-nitrilotriacetic acid-agarose (Qiagen). In-gel cleavage of the EphA5 fusion protein was performed at room temperature by incubating the fusion protein attached to nickel-nitrilotriacetic acid-agarose with thrombin overnight. The released EphA5 protein was further purified on an AKTA FPLC machine (Amersham Biosciences) using a gel filtration column (HiLoad 16/60 Superdex 200) equilibrated in 20 mM sodium phosphate (pH 7.3) containing 150 mM sodium chloride.

For the crystallization of EphA5, the harvested cells were sonicated and protein was purified by gel filtration in 25mM Tris-HCl (pH 7.8), containing 150mM NaCl and 5mM $CaCl_2$. To increase the purity of the EphA5, the eluted fractions from gel filtration step were combined and buffer exchanged to 25mM Tris-HCl (pH 7.8), and then purified by ion-exchange chromatography using anion-exchange column (Mono Q 5/50). The column was eluted with a gradient of NaCl from 0 to 1 M in 25 mM Tris-HCl (pH 7.8). The eluted fraction containing the EphA5 ligand-binding domain was collected and again buffer exchanged to 25 mM Tris-HCl (pH 7.8), containing 150 mM NaCl and 5 mM $CaCl_2$ for storage. The purity of the protein was verified by the SDS-PAGE, and the identity of EphA5 was verified by MALDI-TOF mass spectrometry.

2.4.2 Expression and purification of WDC and its mutants

The recombinant WDC and its mutants were overexpressed in *E. coli* Rosetta-gami (DE3) cells. Briefly, the cells were cultured in Luria-Bertani medium at 37°C until the absorbance at 600 nm reached ~0.6. Isopropyl 1-thio-D-galactopyranoside was then added to a final concentration of 0.5 mM to induce peptides expression at 20°C overnight. The harvested cells were sonicated in lysis buffer containing 20 mM sodium phosphate (pH 7.3) and 150 mM sodium chloride to release soluble GST-tagged peptides, which were subsequently purified with glutathione-Sepharose (Amersham Biosciences). The peptides were released from the GST fusion proteins by in-gel thrombin cleavage followed by HPLC purifications on a RP-18 column (Vydac). The formation of disulfide bridge of WDC and its mutants was determined by both HPLC and MALDI-TOF mass spectrometry.

2.4.3 Preparation of the isotope-labelled protein and/or peptides

The generation of the isotope-labelled protein and peptides for NMR studies followed a similar procedure except that the bacteria were grown in M9 medium with the addition of $(^{15}NH_4)_2SO_4$ for ^{15}N labelling and $(^{15}NH_4)_2SO_4$/[^{13}C]glucose for ^{15}N-/^{13}C double labelling. The concentration of protein and peptides samples was determined by a spectroscopic method (Beer-Lamber Law) in the presence of 6 M guanidine hydrochloride (Pace *et al.* 1995).

2.5 Circular Dichroism (CD) Measurement

The CD spectra of peptides and proteins were recorded in 10 mM phosphate buffer (pH 6.3) on a Jasco J-810 spectropolarimeter equipped with a thermal controller (Liu *et al.* 2006). The samples at a protein concentration of ~20 μM were scanned in a capped quartz cuvette of 1-mm path length in the wavelength range of 260-190 nm at 25°C under nitrogen flush. Data from three independent scans were added and averaged.

2.6 Crystallization of EphA5

The EphA5 ligand-binding domain was prepared at a concentration of 10 mg/ml in a buffer containing 25 mM Tris-HCl (pH 7.8), 150 mM NaCl and 5 mM $CaCl_2$. Crystal screen was set up by preparing 2-μl hanging drops at room temperature in a well containing different reservoir solution. Rock-like crystals formed in the well containing 0.1 M Tris-HCl (pH 8.5) and 2.0 M ammonium sulfate. After careful optimization of the concentration of ammonium sulfate and the pH of Tris-HCl, high quality crystals grew after 3 days under the condition of 0.1 M Tris-HCl (pH 8.5) and 2.0 M ammonium sulfate.

2.7 Characterization of the Binding of EphA5 with WDC and its Mutants by HSQC of NMR

To characterize the binding interaction of WDC and its mutants with EphA5 by NMR, two-dimensional ^{1}H-^{15}N HSQC spectra of the ^{15}N-labeled EphA5 were acquired at a protein concentration of ~100 μM in the absence or presence of WDC and its mutants at different molar ratios. By superimposing the HSQC spectra of the ^{15}N-labeled EphA5 in the absence and presence of peptides, the shifted HSQC peaks could be identified.

Similarly, the binding interaction between WDC and EphA5 was further investigated by monitoring the shifts of HSQC peaks in the spectra of the ~100 μM ^{15}N-labeled WDC peptide upon addition of unlabeled EphA5.

2.8 Characterization of the Binding of EphA5 with WDC and its Mutants by Isothermal Titration Calorimetry (ITC)

All ITC experiments were performed using a Microcal VP ITC machine. Titrations of the binding of WDC and its mutants to EphA5 were conducted in 10 mM phosphate buffer (pH 6.3) and at 25°C. The EphA5 was placed in a 1.8-mL sample cell, while the peptides were loaded into a 300 μL syringe. The samples were degassed for 15 min and spun down for 5 min to remove bubbles before titrations were initiated. A control experiment with the same parameter setting was also performed to subtract the contribution of the peptide dilution. The titration data after the results of the control experiment had been subtracted were fitted using the built-in software ORIGIN to yield the thermodynamic binding parameters.

2.9 NMR Experiments of EphA5 and WDC

2.9.1 Backbone assignment of EphA5

Double-labeled EphA5 (0.5 mM) with or without WDC was prepared in 10 mM phosphate buffer (pH 6.3) with the addition of 10% D_2O for NMR spin-lock. For the preliminary backbone sequential assignment, a pair of triple-resonance NMR spectra, HNCACB and CBCA(CO)NH were collected at 25°C on an 800-MHz Bruker Avance

spectrometer equipped with a shielded cryoprobe. All NMR data were processed with NMRPipe and analyzed with NMRView.

2.9.2 Structure determination of WDC by NMR

A 1.0 mM solution of WDC was prepared in 10 mM phosphate buffer (pH 6.3) with the addition of 10% D_2O for the 2D ^1H TOCSY and NOESY experiments. The NMR spectra were collected at 15°C on an 800-MHz Bruker Avance spectrometer equipped with a shielded cryoprobe. All NMR data were processed with NMRPipe and analyzed with NMRView.

For structure calculation, a set of manually assigned unambiguous NOE restraints extracted from two-dimensional 1H NOESY spectra were input to calculate initial structures with CYANA. With the availability of the initial structure, more NOE crosspeaks in the two NOESY spectra were automatically assigned by CYANA program followed by extensive manual confirmation and correction. After several rounds of refinement, the final set of unambiguous NOE, and disulfide bridge were input for the structure determination by CYANA. The 10 lowest-energy structures accepted by the CNS protocol were checked by PROCHECK and subsequently analyzed by using MolMol.

Chaper III EXPERIMENTAL RESULTS AND DISCUSSIONS

3.1 Expression and purification of EphA5 Ligand-Binding Domain

The recombinant EphA5 was over expressed in *E. coli* Rosetta-gami (DE3) cells to increase the correct formation of disulfide bridge. The released soluble recombinant His-tagged EphA5 proteins were purified by affinity chromatography using nickel-nitrilotriacetic acid-agarose (Qiagen). After in-gel cleavage of the EphA5 fusion protein with thrombin overnight at room temperature, the released EphA5 protein was further purified on an AKTA FPLC machine. The expression of EphA5 and the purity of the purified protein were assessed by SDS-PAGE using 15% gel (Figure 5). Since His-tag has a molecular weight of around 2 kDa, EphA5 without the His-tag migrated faster compared to His-tagged-EphA5 from the beads.

For crystallization, the purity of purified EphA5 was further enhanced by ion-exchange chromatography using an anion-exchange column (Mono Q 5/50). The protein eluted from the Mono Q5/50 column appeared homogenous as determined by SDS-PAGE (data not shown).

3.2 Structural Characterization of EphA5 by CD

After the EphA5 ligand-binding domain was successfully purified by FPLC, its structural property was first assessed by far-UV CD spectroscopy. As shown in Figure 6A, the spectrum of the protein showed a maximal negative signal at ~213 nm. This implied that EphA5 is a typical β-protein (Figure 6A). To see the overall tertiary packing of EphA5, the near-UV CD spectra of EphA5 in the absence and presence of 6 M

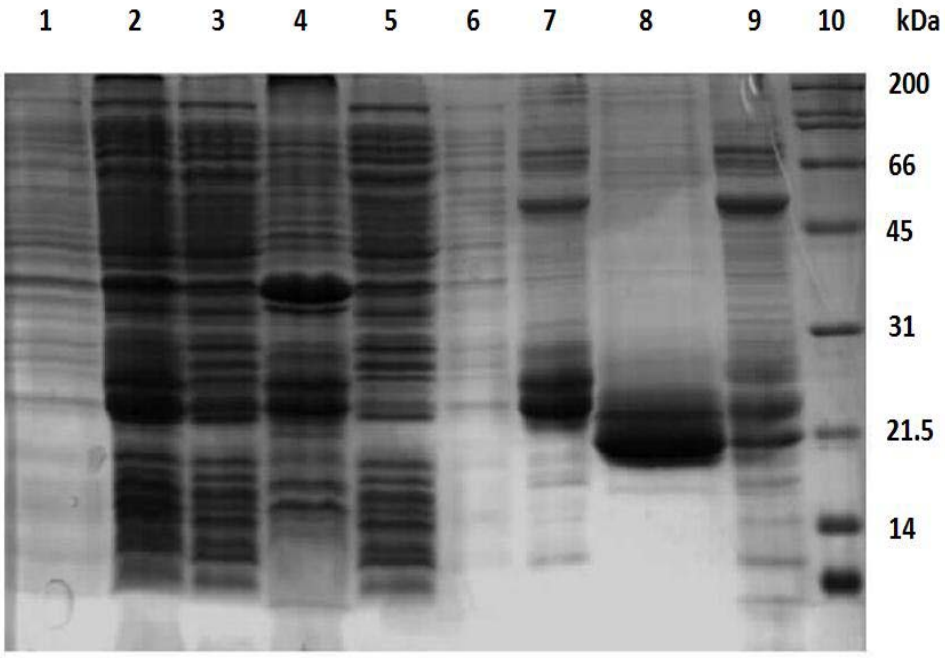

Figure 5: Samples of EphA5 receptor on a 15% SDS-PAGE gel. Lane 1, Total cell extract before induction. Lane 2, Total cell extract with a 0.1 mM isopropyl-1-thio-b-D-galactopyranoside induction at 20°C for overnight; Lane 3, Supernatant of the cell lysate solubilised in the PBS buffer (pH 7.3); Lane 4, Pellet of the cell; Lane 5, Flow-through fraction after passing through Ni^{2+}-affinity column; Lane 6, Flow-through fraction from extensive washing with PBS buffer (pH 7.3); Lane 7, Ni^{2+}-agarose beads after an extensive PBS buffer-washing; Lane 8: Elution of EphA5 receptor after overnight in-gel cleavage by thrombin; Lane 9: Ni^{2+}-agarose beads after thrombin cleavage; Lane 10: Protein markers.

guanidinium chloride were recorded (Figure 6B). The near-UV CD spectra showed that without the denaturant guanidinium chloride, EphA5 adopted tight tertiary packing, a property that was lost under denaturation condition.

Moreover, thermal unfolding study for EphA5 was conducted and the result indicated the existence of a relatively cooperative unfolding transition from 55 to 75°C (Figure 6C, D). However, EphA5 still had a far-CD spectrum with a maximal negative signal at ~215 nm at 95°C, which implied that thermal unfolding was insufficient to completely denature EphA5 even at a temperature as high as 95°C.

3.3 Crystal Structure of EphA5 Ligand-Binding Domain

The EphA5 ligand-binding domain purified by anion-exchange chromatography was crystallized under the condition of 0.1 M Tris-HCl (pH 8.5) and 2.0 M ammonium sulfate. The crystal structure of EphA5 ligand-binding domain was determined by the Molecular Replacement method using EphA4 ligand-binding domain as a search model. The crystal structure was refined at 2.6 Å resolution with a final *R*-factor of 0.2049 (R_{free}=0.2824). The atomic coordinates were deposited in the Protein Data Bank with the PDB ID of 3DLY. The EphA5 ligand-binding domain exhibited both the conserved jellyroll folding architecture and a compact β-sandwich (Figure 7). The jellyroll consists of 11 anti-parallel β-sheets connected by loops of varying length and two disulfide bonds.

3.4 Structural Characterization of EphA5 by NMR

To acquire more structural information of EphA5, and its characterization in

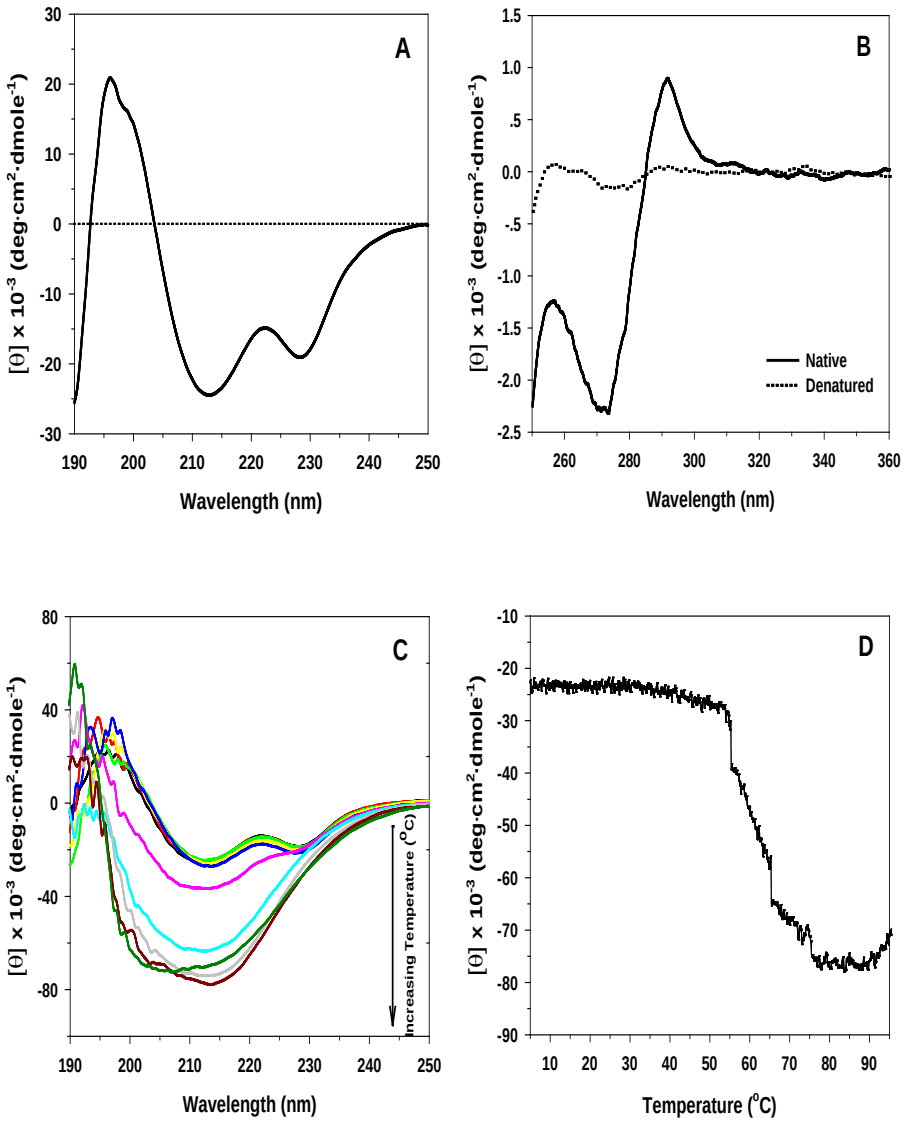

Figure 6: Preliminary structural characterization of EphA5 by CD. (A) Far-UV CD spectrum of 20 µM EphA5 in the 10 mM phosphate buffer (pH 6.3). (B) Near-UV CD spectra of 20 µM EphA5 in 10 mM phosphate buffer (pH 6.3) without (black line) and with 6 M guanidinium chloride (dash line). (C) Far-UV CD spectra of EphA5 during the thermal unfolding process from 5 to 95℃. (D)The thermal unfolding curve monitored at 216 nm.

Figure 7: Crystal structure of the EphA5 ligand-binding domain.

solution, HSQC spectrum of EphA5 was obtained (Figure 8). EphA5 had a well-dispersed HSQC spectrum with 4.1ppm for ^{1}H dimension and 28.1ppm for ^{15}N dimension, respectively. This result indicated that EphA5 protein had a well-packed tertiary structure as confirmed by the data from CD spectra. Therefore, NMR would be suitable for studying the structure of EphA5 and binding affinity of EphA5 for ligands.

3.5 Characterization of Binding Interactions between EphA5 and WDC Peptide by NMR

The NMR titration was used to determine the binding affinity between EphA5 and WDC peptide. Two-dimensional ^{1}H-^{15}N HSQC spectrum of ~100 μM ^{15}N-labeled EphA5 in10 mM phosphate buffer (pH 6.3) at 25 °C was first recorded with an 800 MHz Bruker NMR spectrometer. After successive addition of WDC, the ^{1}H-^{15}N HSQC spectra of ^{15}N-labeled EphA5 were then recorded again in the same parameters.

At a molar ratio of 1:1, two sets of the HSQC peaks were observed for almost all residues of the EphA5 ligand-binding domain. One set which represented the free EphA5 had no peak shift, whereas the other set which represented the EphA5-WDC peptide complexes showed extensive peak shifts. When the molar ratio of EphA5 to WDC reached 1:3, the HSQC peak set from the free ^{15}N-labeled EphA5 all shifted to become identical with the set from the complexes of EphA5 and WDC (Figure 9A). After further addition of WDC to a molar ratio of 1:4, the HSQC peaks did not exhibit significant further shift, indicating that the binding of EphA5 with WDC had become saturated (data not shown).

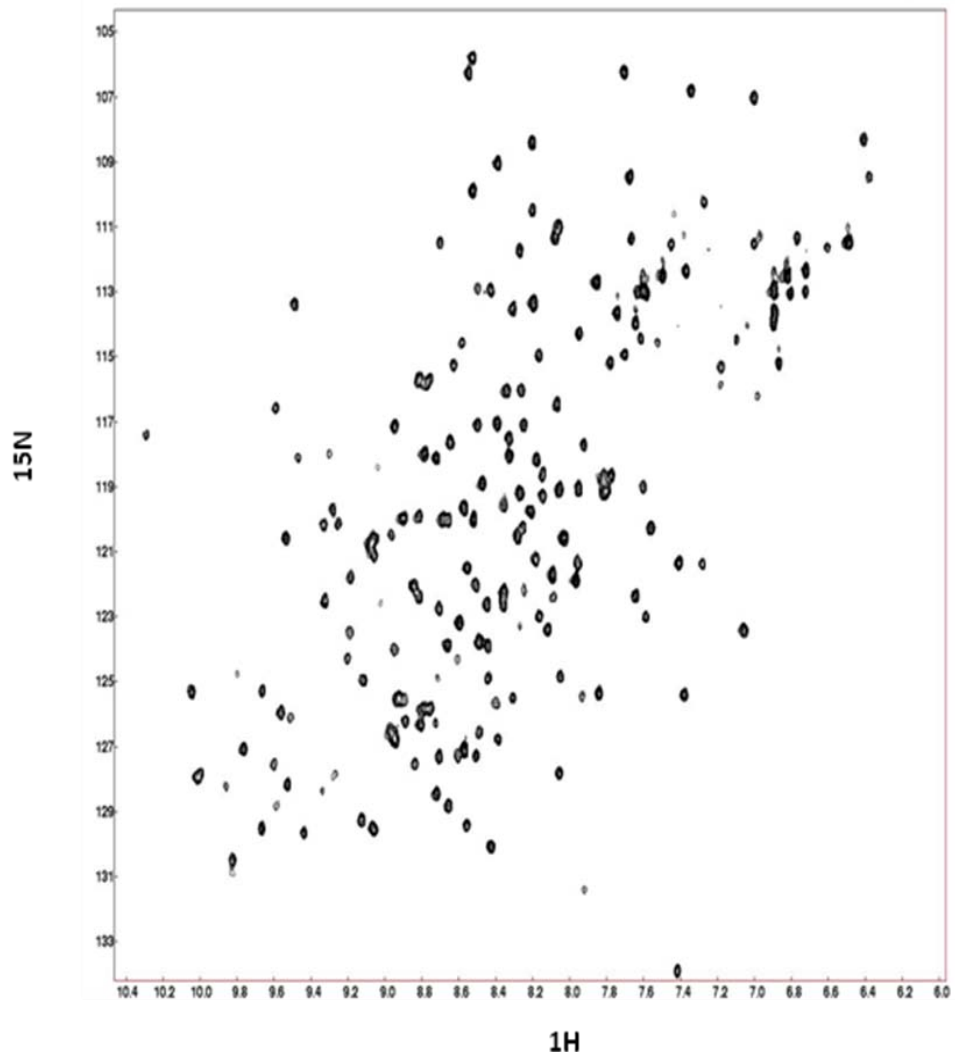

Figure 8: ^{1}H-^{15}N HSQC spectrum of the EphA5 ligand-binding domain.

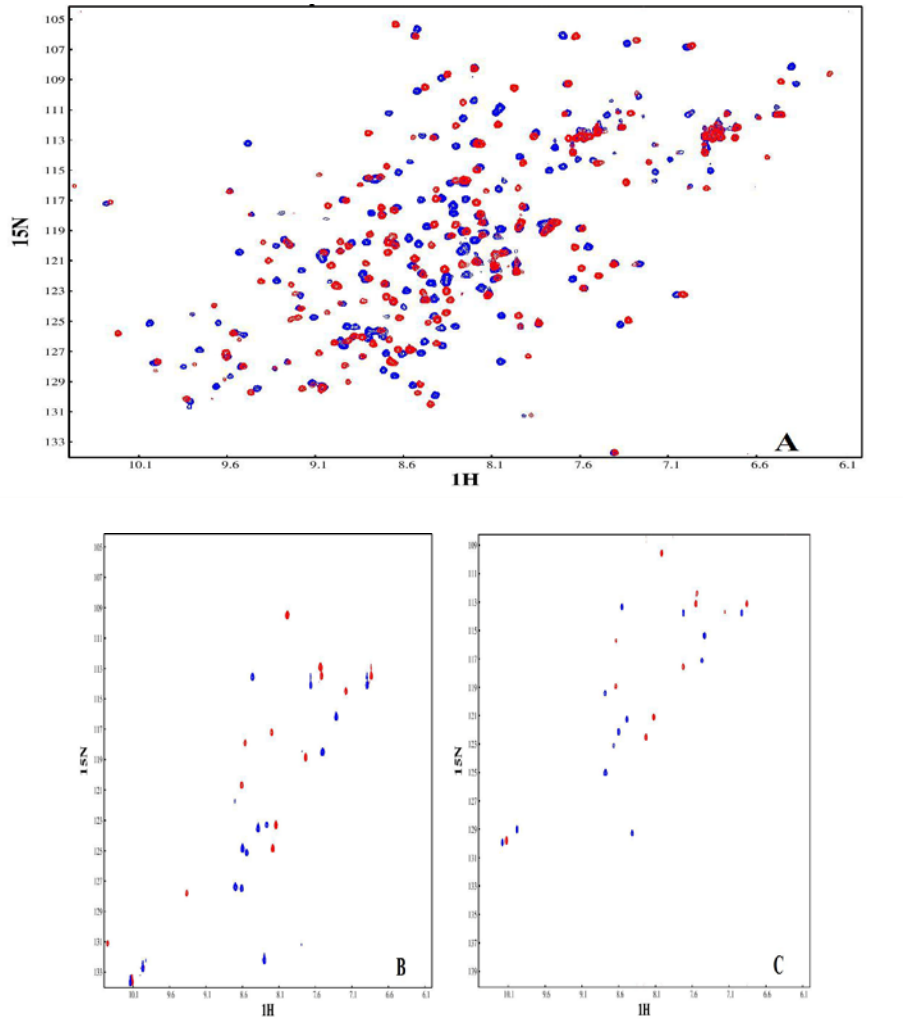

Figure 9: NMR characterization of the binding between EphA5 and WDC. (A) Superimposition of the HSQC spectra of the ^{15}N-labeled EphA5 in the absence (blue) and presence (red) of WDC at a molar ratio of 1:3. (B) Superimposition of the HSQC spectra of the ^{15}N-labeled WDC in the absence (blue) and presence (red) of EphA5 at a molar ratio of 1:3. Both spectra were acquired in 10 mM phosphate buffer (pH 6.3) at 25 °C using an 800 MHz Bruker NMR spectrometer. (C) Superimposition of the HSQC spectra of the ^{15}N-labeled WDC in the absence (blue) and presence (red) of EphA5 at a molar ratio of 1:3. Spectra were acquired in 10 mM phosphate buffer (pH 6.3) at 15°C using an 800 MHz Bruker NMR spectrometer.

Meanwhile, the binding interaction between EphA5 and WDC was further investigated by monitoring the shifts of HSQC peaks of the ~100 μM ^{15}N-labeled WDC peptide upon successive additions of unlabeled EphA5. Similarly, at a WDC to EphA5 molar ratio of 1:3, the HSQC peak set from the free ^{15}N-labeled WDC all shifted to become identical with the set from the complexes of EphA5 and WDC at both 25°C and 15°C (Figure 9B and C).

3.6 Characterization of Binding Interactions between EphA5 and WDC Peptide by ITC

To analyze the binding affinity of the EphA5 ligand-binding domain for WDC, ITC was utilized to measure their thermodynamic binding parameters. Figure 10 presented the ITC profile for the interaction of EphA5 with WDC at 25°C. After the profile was fitted by ORIGIN software, the thermodynamic parameters were obtained as shown in Table 2. The K_d for the binding of EphA5 with WDC was 6.22 μM, which indicated that the binding between EphA5 and WDC was of medium affinity.

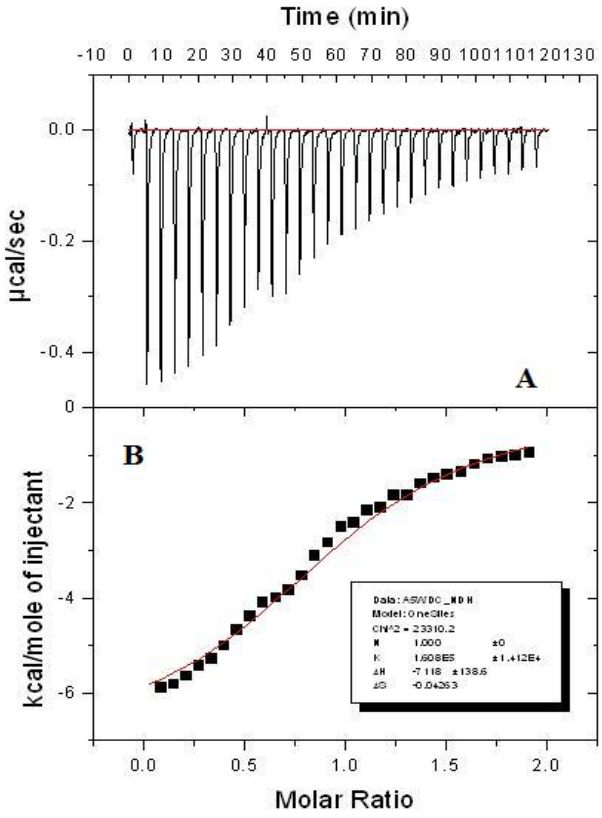

Figure 10: ITC characterization of the binding between EphA5 and WDC. (A) ITC titration profiles of the binding reaction between EphA5 and WDC. (B) Integrated values for reaction heat with subtraction of the corresponding blank results normalized by the amount of ligand injected versus WDC/EphA5 molar ratio. The detailed conditions and setting of the ITC experiments are presented in Materials and Methods as well as in Table 2.

Table 2: Thermodynamic parameters of the binding interactions between EphA5 receptor with WDC and its two mutants

Syringe	Cell	Temp (°C)	Injection Volume (µL)	K_a (M^{-1})	K_d (µM)	Δ*S*	Δ*H*
WDC (500 µM)	EphA5 (28 µM)	25	5	$1.608\times10^5\pm1.412\times10^4$	6.22	-0.04263	-7118±138.6
1WA (500 µM)	EphA5 (28 µM)	25	5	$2.595\times10^5\pm1.557\times10^4$	3.85	-1.653	-7750±89.05
4NA (500 µM)	EphA5 (25 µM)	25	5	$0.891\times10^5\pm0.522\times10^4$	11.22	-1.201	-6995±122.5

3.7 Structural Characterization of WDC by CD

HPLC-purified WDC peptide was dried by lyophilization for two days. The formation of disulfide bridge in WDC was confirmed by HPLC (Figure 11) and by MALDI-TOF mass spectrometry (Figure 12).

As shown in the Figure 11, native WDC showed one peak in the HPLC profile, whereas WDC denatured by 8 M urea and 100 mM DTT showed two peaks. The first peak possessed the same retention time as native WDC, and the second peak had a ~1 min delayed retention time, which implied the disulfide bridge of WDC had been disrupted by 100 mM DTT. Mass spectroscopy analysis of WDC yielded a molecular weight of 1592.5 Da, which was consistent with its calculated value of 1592.7 Da (Figure 12).

The structural property of WDC was first investigated by far-UV CD spectroscopy in 10 mM phosphate buffer (pH 6.3) at 25°C. As shown in Figure 13A, the far-UV spectrum of WDC has a maximal negative signal at ~212 nm, which indicated the presence of β strand structure, formed as a result of the presence of disulfide bridge between Cys^5 and Cys^{10}.

Moreover, the result from thermal unfolding study of WDC showed that the CD spectra of WDC shifted to a maximal negative peak at ~201nm at a temperature of 75°C or higher, which implied that WDC had become unstructured (Figure 13 B and C).

3.8 Structural Characterization of WDC by NMR

To explore the structural properties of WDC, NMR spectroscopy was further utilized. ^{1}H-^{15}N HSQC spectrum of ^{15}N-labeled WDC at 15°C (Figure 14A) showed that

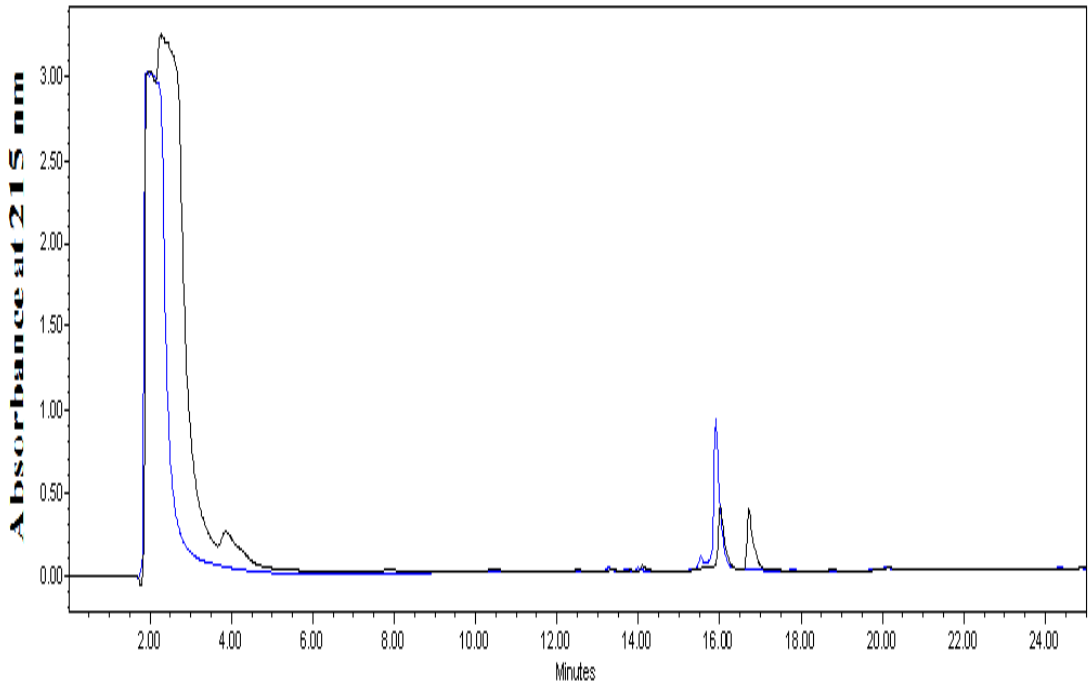

Figure 11: Comparison of retention time between native and denatured WDC on an analytic RP-18 column. Blue line: WDC in 10 mM phosphate buffer (pH 6.3); Black line: WDC denatured in 8 M urea and 100 mM DTT plus 10 mM phosphate buffer (pH 6.3) for 1 hr at room temperature.

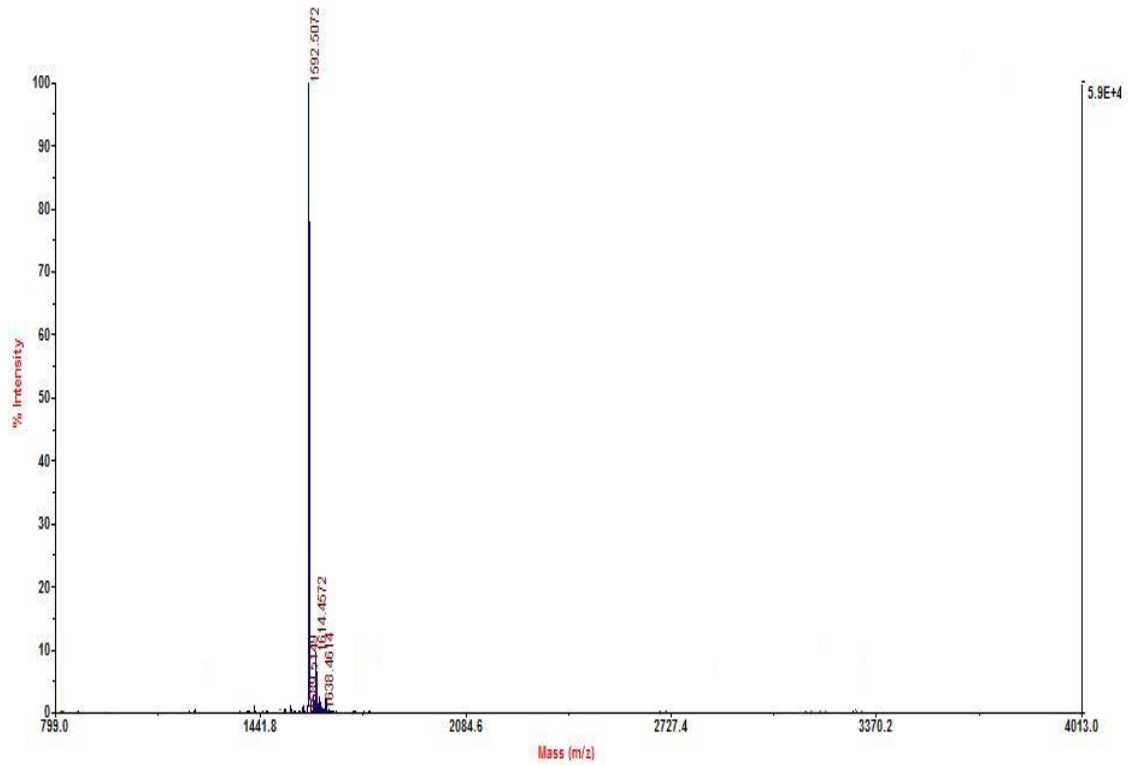

Figure 12: MALDI-TOF mass spectrum of WDC. Peptide was desalted and re-dissolved in water. The calculated MW of WDC was 1592.7 Da and the determined MW of WDC was 1592.5 Da.

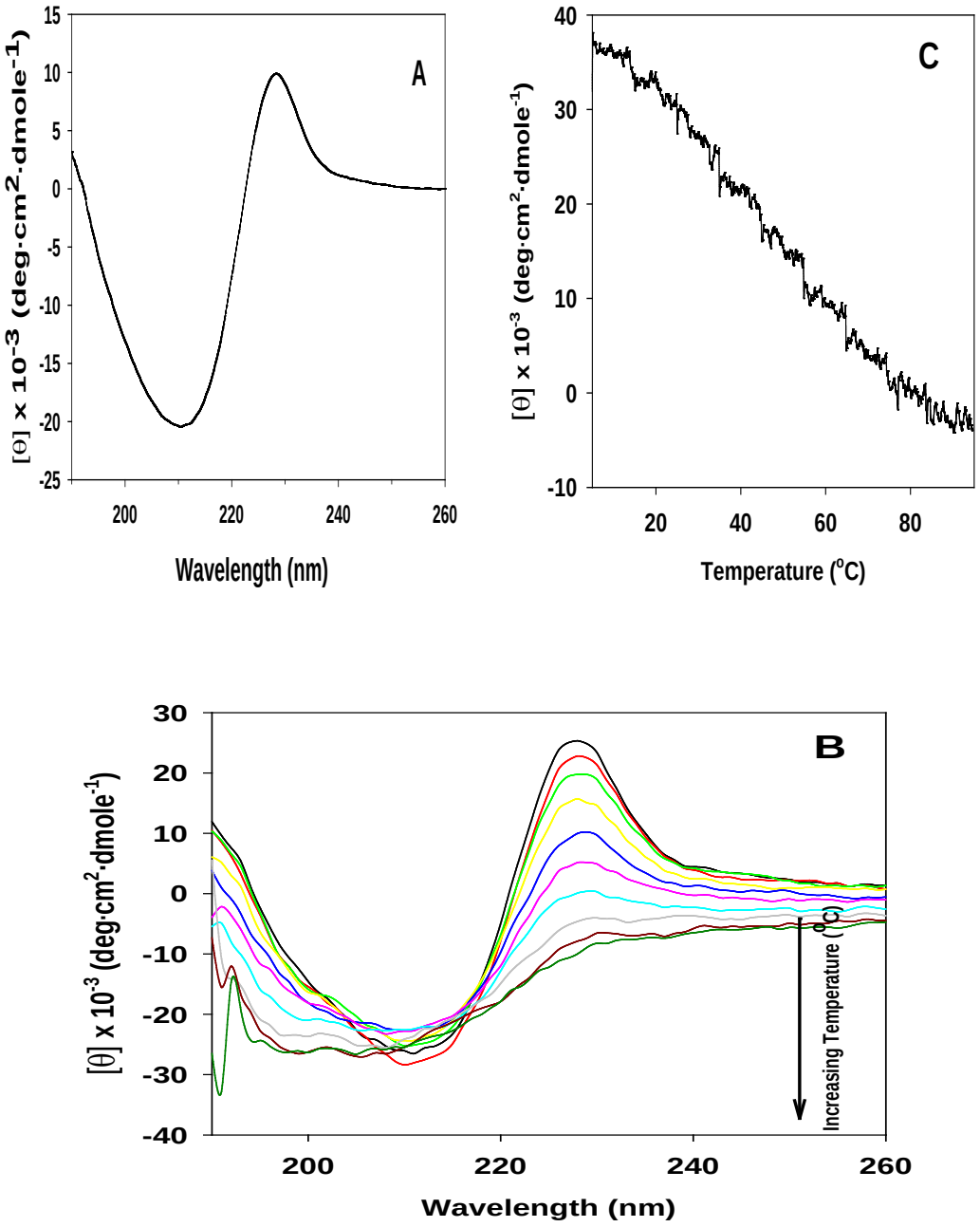

Figure 13: Preliminary structural characterization of WDC by CD. (A) Far-UV CD spectrum of 50 µM WDC in the 10 mM phosphate buffer (pH 6.3). (B) Far-UV CD spectra of WDC collected at a 10˚C interval during the thermal unfolding from 5 to 95˚C. (C) The thermal unfolding curve monitored at 216 nm.

peaks from all amino acid except Gly^1 were visible. Therefore, it was possible to assign all amino acids of WDC.

To obtain better spectra, both TOCSY and NOESY spectra were acquired not at 25°C but at 15°C in 10 mM phosphate buffer (pH 6.3). The mixing time in NOESY spectrum was 75 ms (Figure 14B).

As the binding of WDC by EphA5 was saturated at a WDC to EphA5 molar ratio of 1:3 at both 25°C and 15°C, the binding between WDC and EphA5 appeared not to be significantly affected by temperature (Figures 9B and C). Furthermore, WDC had similar CD spectra in both 25°C and 15°C, which showed that temperature had no significant effect on its structure.

3.9 NMR Structure of WDC

2D ^1H TOCSY and NOESY experiments of 1mM WDC in 10 mM phosphate buffer (pH 6.3) were first collected at 15°C on an 800-MHz Bruker Avance spectrometer equipped with a shielded cryoprobe. All NMR data were then processed with NMRPipe and analyzed with NMRView.

According to TOCSY and NOESY spectra, the preliminary sequential assignment was completed. The assigned ^1H chemical shifts of WDC were presented in Table 3. The NMR structure of WDC was further calculated from the NOE restraints by CAYNA program, and 10 lowest-energy accepted structures were selected after several rounds of refinement. The 10 selected NMR structures of WDC in solution are showed in Figure 15. Superimposition of the 10 selected NMR structures of WDC over the backbone atoms

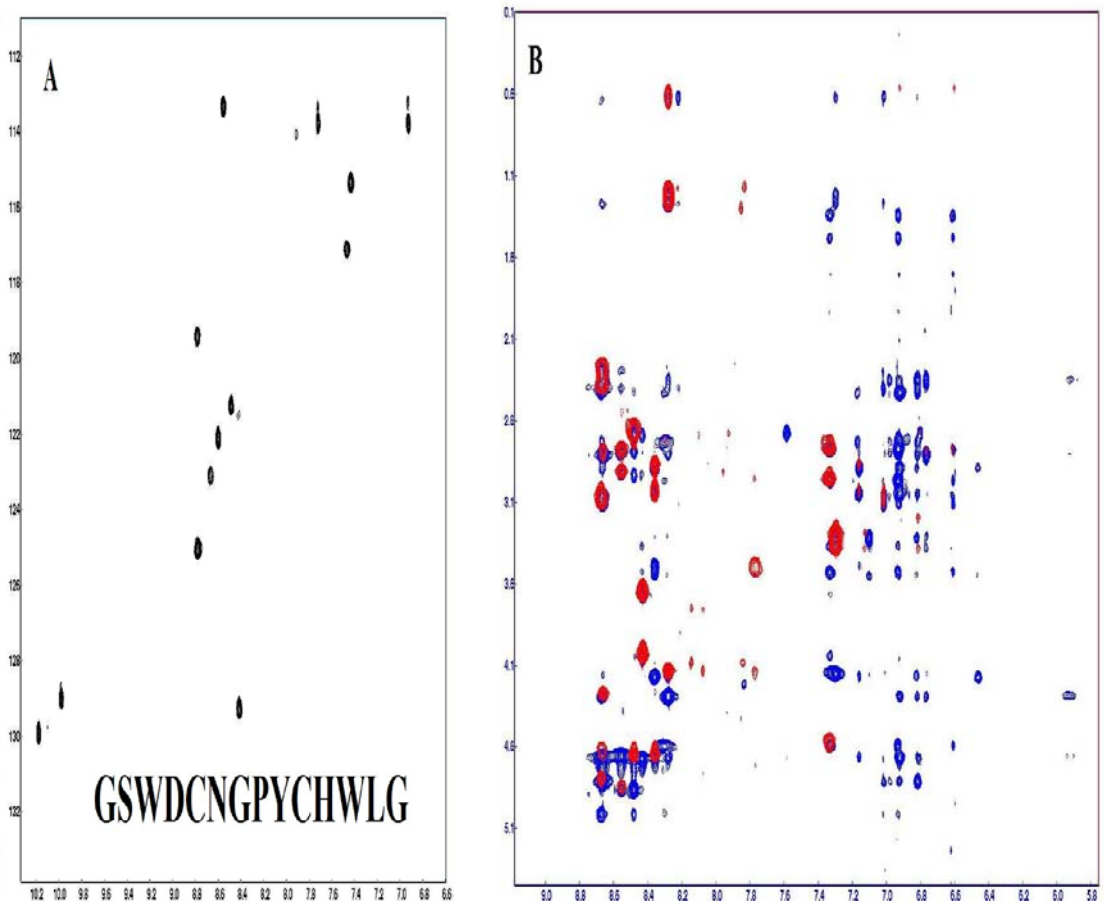

Figure 14: NMR characterization of WDC. (A) HSQC spectrum of the ^{15}N-labeled WDC acquired in 10 mM phosphate buffer (pH 6.3) at 15°C on an 800 MHz Bruker NMR spectrometer. (B) NH-aliphatic region spectra of TOCSY (red) and NOESY (blue) acquired in 10 mM phosphate buffer (pH 6.3) at 15°C on an 800 MHz Bruker NMR spectrometer (Mixing time for NOESY is 75 ms).

Table 3: Chemical shift of WDC in 10 mM phosphate buffer (pH 6.3) at 15˚C

NO	Residue	NH	Hα	Hβ	Hγ	Hδ	other
1	**Gly**						
2	**Ser**	7.774	4.138	3.488 3.519			
3	**Trp**	8.361	4.656	2.872 3.033			7.162, 10.048 6.462, 6.820
4	**Asp**	8.669	4.633	2.274 2.386			
5	**Cys**	8.554	4.843	2.801 2.935			
6	**Asn**	8.48	4.65	2.653 2.687			6.808 7.589
7	**Gly**	8.429	3.666 4.047				
8	**Pro**		4.136	1.693 1.928	1.317 1.467	3.368 3.534	
9	**Tyr**	7.34	4.558	2.776 2.962			6.61 6.92
10	**Cys**	8.302	5.013	2.411 2.716			
11	**His**	8.675	4.795	3.05 3.093			7.019 8.22
12	**Trp**	8.662	4.277	2.338 2.788			6.767, 9.851 7.104, 5.923 6.931, 6.606
13	**Leu**	8.279	4.125	1.181 1.272		0.588 0.631	
14	**Gly**	7.301	3.291 3.384				

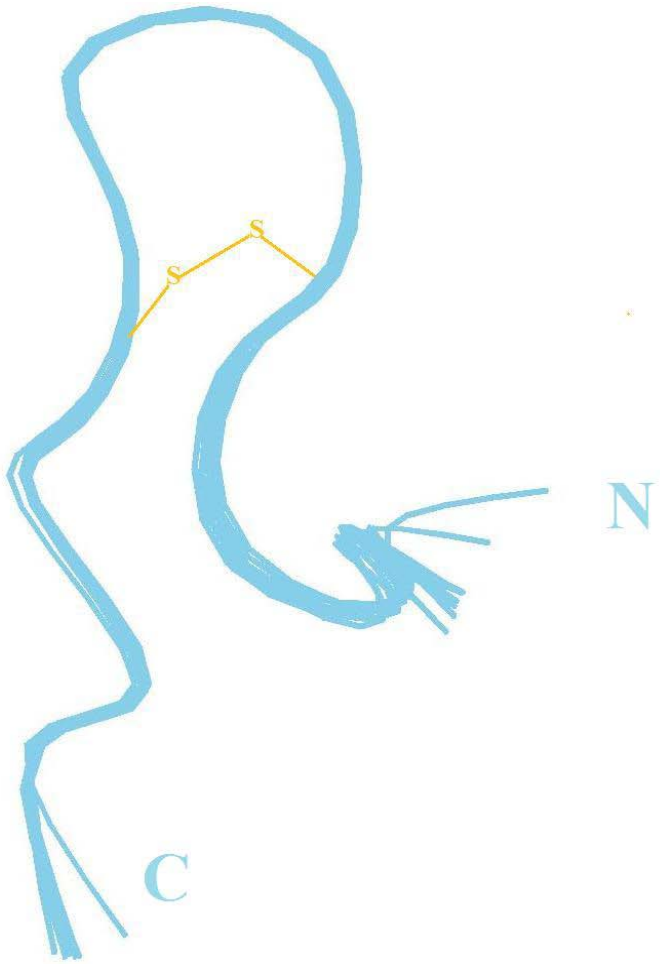

Figure 15: Structures of WDC in the ribbon mode as determined by NMR.

revealed root mean squared deviations (RMSD) of 0.33 ± 0.15 Å for the backbone atoms (N, C_α, C', O) and 0.53 ± 0.07 Å for all heavy atoms from mean structures.

WDC has a single disulfide bridge (Cys^5-Cys^{10}) forming a 4-residue ring, in which the presence of Gly^6 and Pro^7 assists with the formation of a β-turn, since Gly and Pro are generally believed to be present at the β-turn (Figure 15).

In order to determine the structure of WDC in the presence of EphA5, 3D HSQC-TOCSY and NOESY experiments were performed with 1mM ^{15}N-WDC in 10 mM phosphate buffer (pH 6.3) in the presence of EphA5 at a WDC to EphA5 molar ratio of 1:3. Spectra were collected at 15°C on an 800-MHz Bruker Avance spectrometer equipped with a shielded cryoprobe. Unfortunately, it was not possible to finish the sequential assignment after the NMR data were processed, because many ^{1}H signal of WDC in the complex with EphA5 were not visible (data not shown).

3.10 Mapping of Binding Interface between EphA5 and WDC by NMR

All the above data showed that WDC can bind with EphA5 receptor with medium affinity. It was of interest to study the surface the EphA5 ligand-binding domain and WDC where binding actually occurs. As attempts to co-crystallize EphA5 with WDC were not successful, NMR spectroscopy was used to map the binding interface between EphA5 receptor and WDC peptide.

3.10.1 Mapping of EphA5-binding interface within WDC by NMR and ITC

3.10.1.1 Interaction of WDC-mutant peptides with EphA5 by NMR

To map the residues within WDC that are involved in the binding of EphA5, the binding interactions between EphA5 and eight WDC-mutant peptides were studied by HSQC titrations (Figure 16). All amino acids in WDC, except for glycine and cysteine, were mutated by an alanine site-directed mutagenesis screen. The peptides sequences of all these mutants are shown in Table 1.

Two dimensional ^{1}H-^{15}N HSQC spectra of the ^{15}N-labeled EphA5 receptor were acquired in the absence and presence of peptides at different EphA5 to peptide molar ratios. For 1WA (Figure 16A) and 4NA (Figure 16C) peptides, their binding interaction with EphA5 were the same as that between EphA5 and WDC. At a molar ratio of 1:1, two sets of the HSQC peaks were observed for almost all the residues of the EphA5 ligand-binding domain. When the molar ratio of EphA5/peptide reached 1:3, the HSQC peak set from the free ^{15}N-labeled EphA5 all shifted to merge with the set from the complexes of EphA5 and WDC. At a molar ratio of 1:4, the binding of EphA5 to these two WDC-mutant peptides was saturated. These results showed that replacement of Trp^{3} and Asn^{6} with Ala did not significantly affect the binding between WDC and EphA5, and implied that Trp^{3} and Asn^{6} in WDC may not be involved in the binding surface for EphA5 receptor.

However, no detectable perturbation of the HSQC peak was observed even at an EphA5 to peptide molar ratio of 1:10 for 2DA (Figure 17B), 6PA (Figure 17D), 7YA (Figure 16E), 9HA (Figure 16F), 10WA (Figure 16G) and 11LA (Figure 16H) peptides. These results implied that Asp^{4}, Pro^{8}, Tyr^{9}, His^{11}, Trp^{12}, and Leu^{13} could play a very important role for the binding of WDC to EphA5 receptor. Therefore, no further ITC study was conducted for these six WDC-mutant peptides.

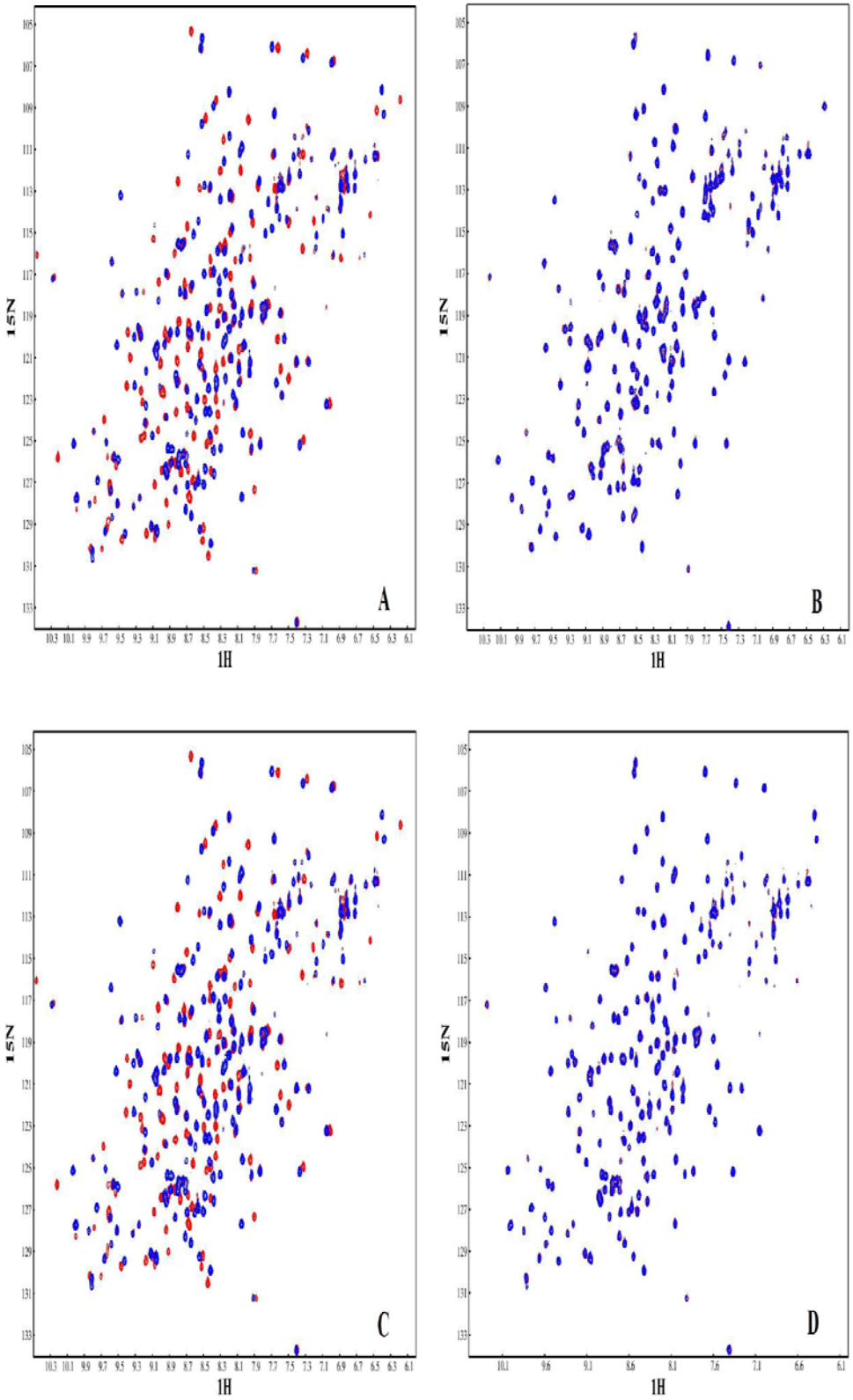
15N
1H
A
B
C
D

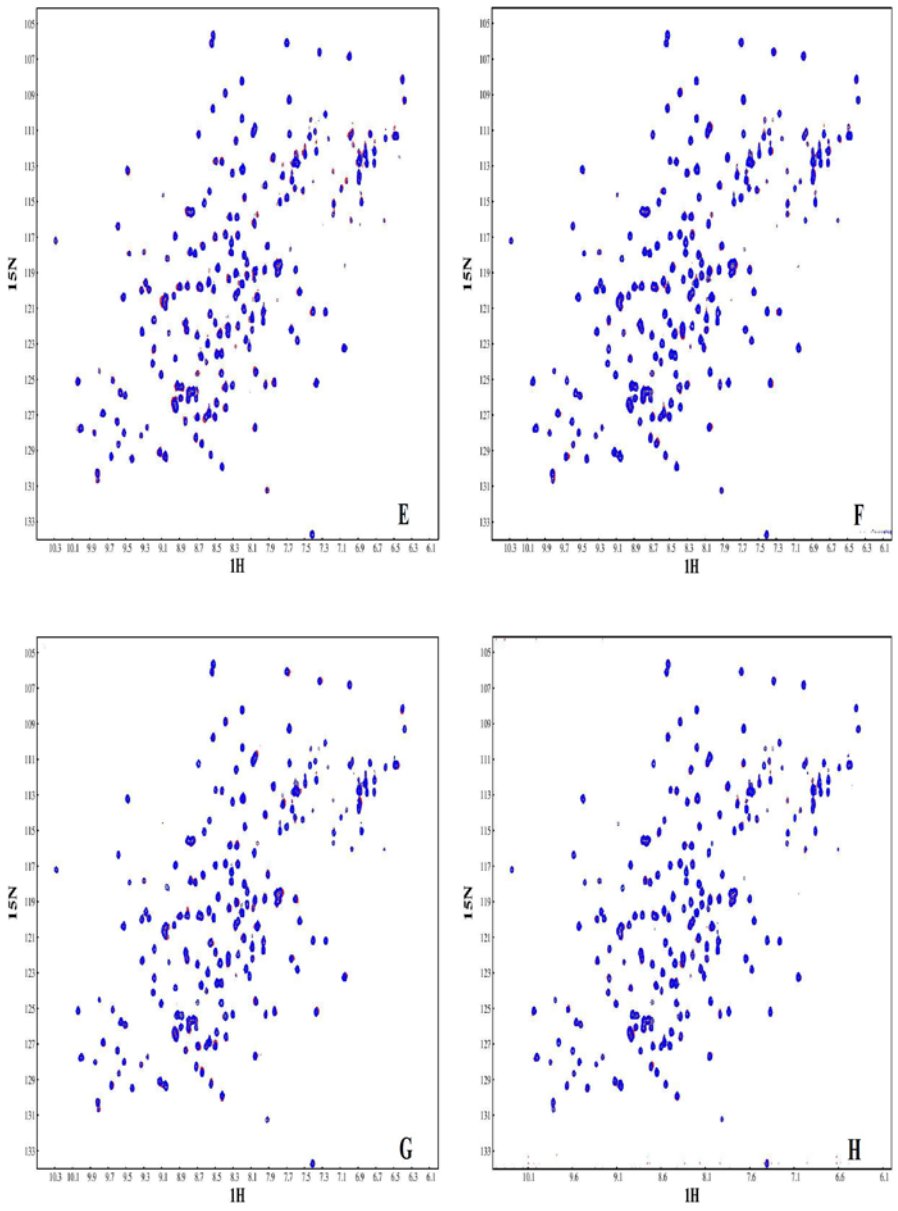

Figure 16: Characterization of the binding between ^{15}N-labeled EphA5 and WDC mutant peptides as determined by NMR. Superimposition of HSQC spectra for the ^{15}N-labeled EphA5 in the absence (blue) and presence (red) of WDC mutant peptides at a different molar ratios. All spectra were acquired in 10 mM phosphate buffer (pH 6.3) except 2DA (pH 5.6) at 25°C on an 800 MHz Bruker NMR spectrometer. (A) 1WA; (B) 2DA; (C) 4NA; (D) 6PA; (E) 7YA; (F) 9HA; (G) 10WA; (H) 11LA.

3.10.1.2 Interaction of WDC-mutant peptides with EphA5 by ITC

The thermodynamic binding parameters of the EphA5 ligand-binding domain with 1WA and 4NA were analyzed by ITC at 25°C. As shown in Figure 17 and Table 2, K_d for the binding between EphA5 and 1WA and between EphA5 and 4NA were 3.85 μM and 11.22 μM, respectively, which is consistent with the K_d for the binding of EphA5 with WDC. Again, it demonstrated that Trp^3 and Asn^6 in WDC may not be involved in the binding WDC to EphA5 receptor.

Taken together, Asp^4, Pro^8, Tyr^9, His^{11}, Trp^{12}, and Leu^{13} in WDC could play a very important role in its binding to EphA5 receptor. To clearly show these binding sites, all side chains of Asp^4, Pro^8, Try^9, His^{11}, Trp^{12} and Leu^{13} are shown in red colour in a stick mode in Figure 18.

3.10.1.3 Structural comparison of WDC and its mutant peptides by CD

To gain insight into the globular secondary structural changes in WDC caused by the Ala site-directed mutagenesis, far-UV CD spectra of all eight WDC-mutant peptides and native WDC were collected. All CD spectra were collected at pH 6.3 and 25°C in 10 mM phosphate buffer except for 2DA, whose CD spectrum was collected at pH 5.6.

It was interesting to notice that except for 1WA and 10WA, in which one of the Trp was replaced by Ala, all six WDC-mutant peptides had same CD spectrum as WDC (Figure 19). Comparison of the spectra of 1WA and 10WA against the spectrum of native WDC indicated that a positive peak around 225 nm disappeared in the spectra of both mutant peptides. However, it was hard to conclude whether the substitution of Trp with

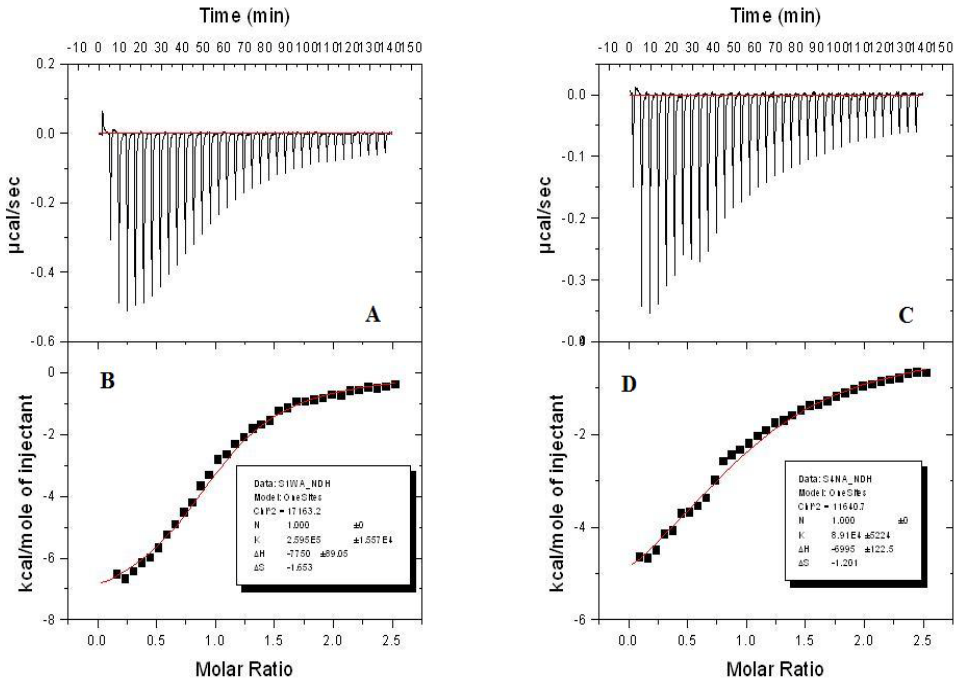

Figure 17: Characterization of the binding between EphA5 and WDC mutant peptides as determined by ITC. ITC titration profiles of the binding reactions of the 1WA (A) and 4NA (C) with EphA5. Integrated values for reaction heats with subtraction of the corresponding blank results normalized by the amount of ligand injected versus 1WA:EphA5 (B) and 4NA:EphA5 (D) molar ratio. The detailed conditions and settings of the ITC experiments were as described in Materials and Methods and Table 2.

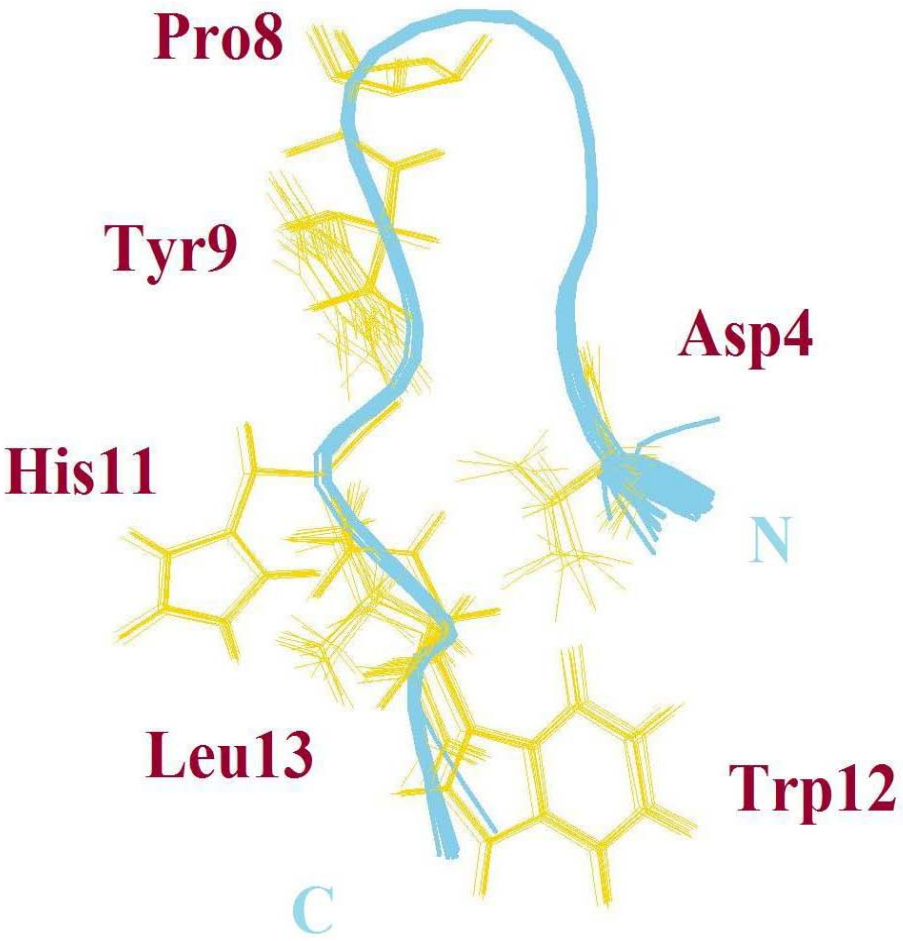

Figure 18: NMR Structures of WDC in the ribbon mode with labelled side chains. The side chains of Asp[4], Pro[8], Try[9], His[11], Trp[12] and Leu[13] were displayed in stick mode and coloured red.

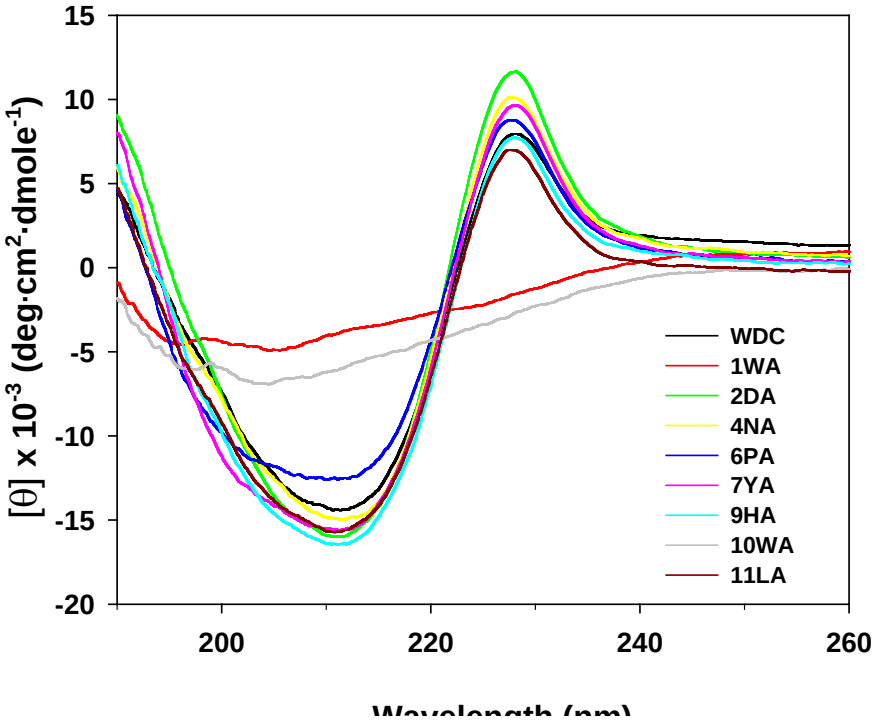

Figure 19: Preliminary structural characterization of WDC and its mutants by CD. Far-UV CD spectra of 50 µM peptides in the 10 mM phosphate buffer (pH 6.3), except 2DA (pH 5.6).

Ala had significantly affected the secondary structure of peptides as the negative band around 225 nm could be caused either by the tryptophan side chains or turn structures (Nagpal *et al.* 1999).

Further study of the effect of mutation on the structure of WDC would require the acquisition of 2D ^{1}H TOCSY and NOESY NMR spectra for these mutant peptides.

3.10.2 Mapping of EphA5-binding interface to WDC by NMR

3.10.2.1 Backbone sequential assignment of EphA5 without and with WDC

^{15}N/^{13}C double-labelled EphA5 of 0.5 mM concentration were prepared in 10 mM phosphate buffer (pH 6.3). A pair of triple-resonance NMR spectra, HNCACB and CBCA(CO)NH was collected at 25°C to obtain the preliminary backbone sequential assignment for EphA5 in the absence and presence of WDC (a WDC to EphA5 molar ratio of 1:3), respectively. The ^{1}H-^{15}N HSQC spectra of assigned EphA5 backbone peaks in the absence and presence of WDC are shown in Figure 20 and Figure 21, respectively.

To evaluate whether the sequential assignment was correct, both Cα and Cβ conformational shifts were calculated. Figure 22 shows that the conformation of β-strands in EphA5 was consistent with the determined conformation obtained by X-ray crystallography. Furthermore, the completed NMR sequential assignments for the EphA5 ligand-binding domain in the absence and presence of WDC indicated that binding of WDC to EphA5 did not induce significant change to the secondary structure of EphA5 (Figure 22).

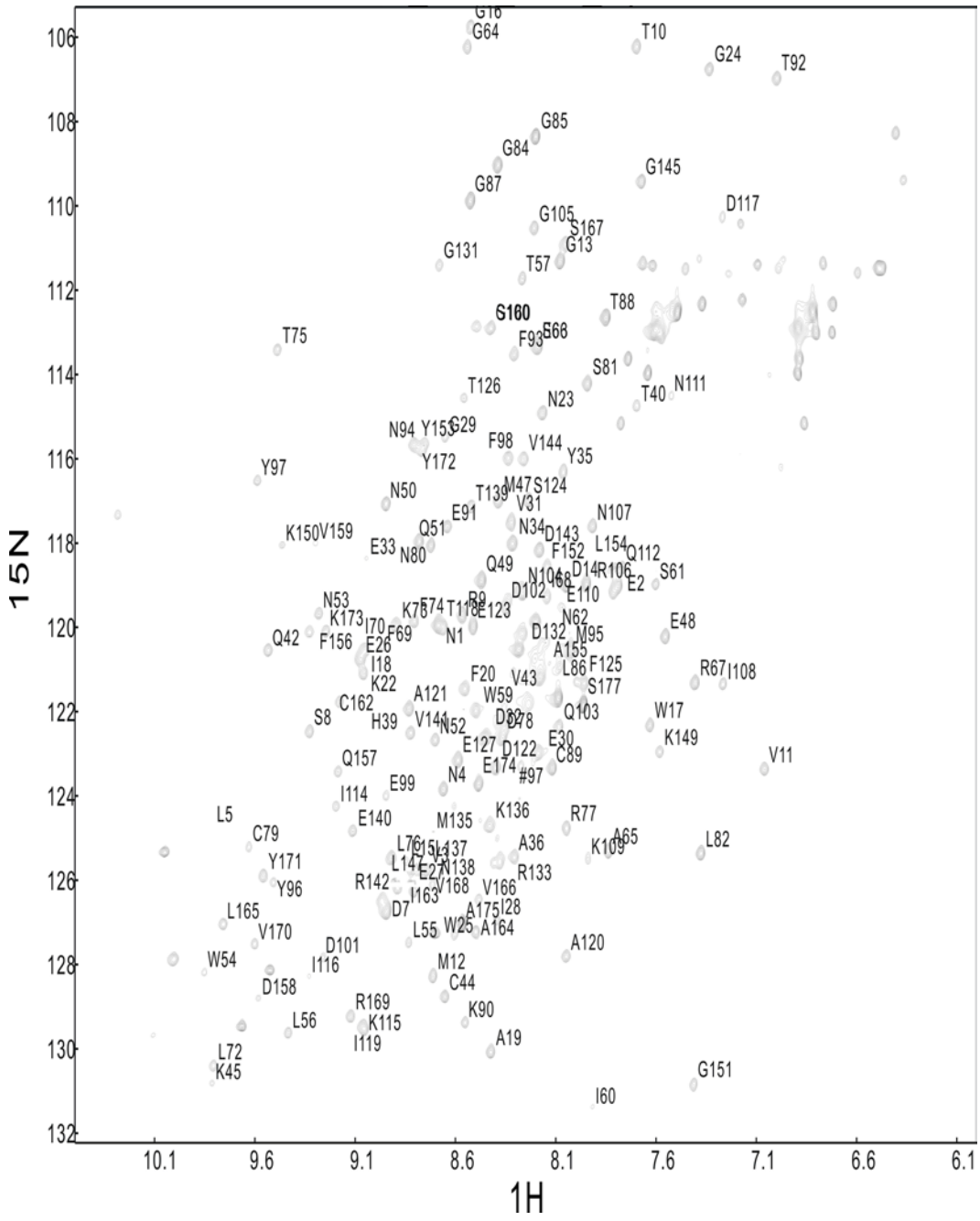

Figure 20: Assigned ^{1}H-^{15}N HSQC spectrum of the EphA5 ligand-binding domain.

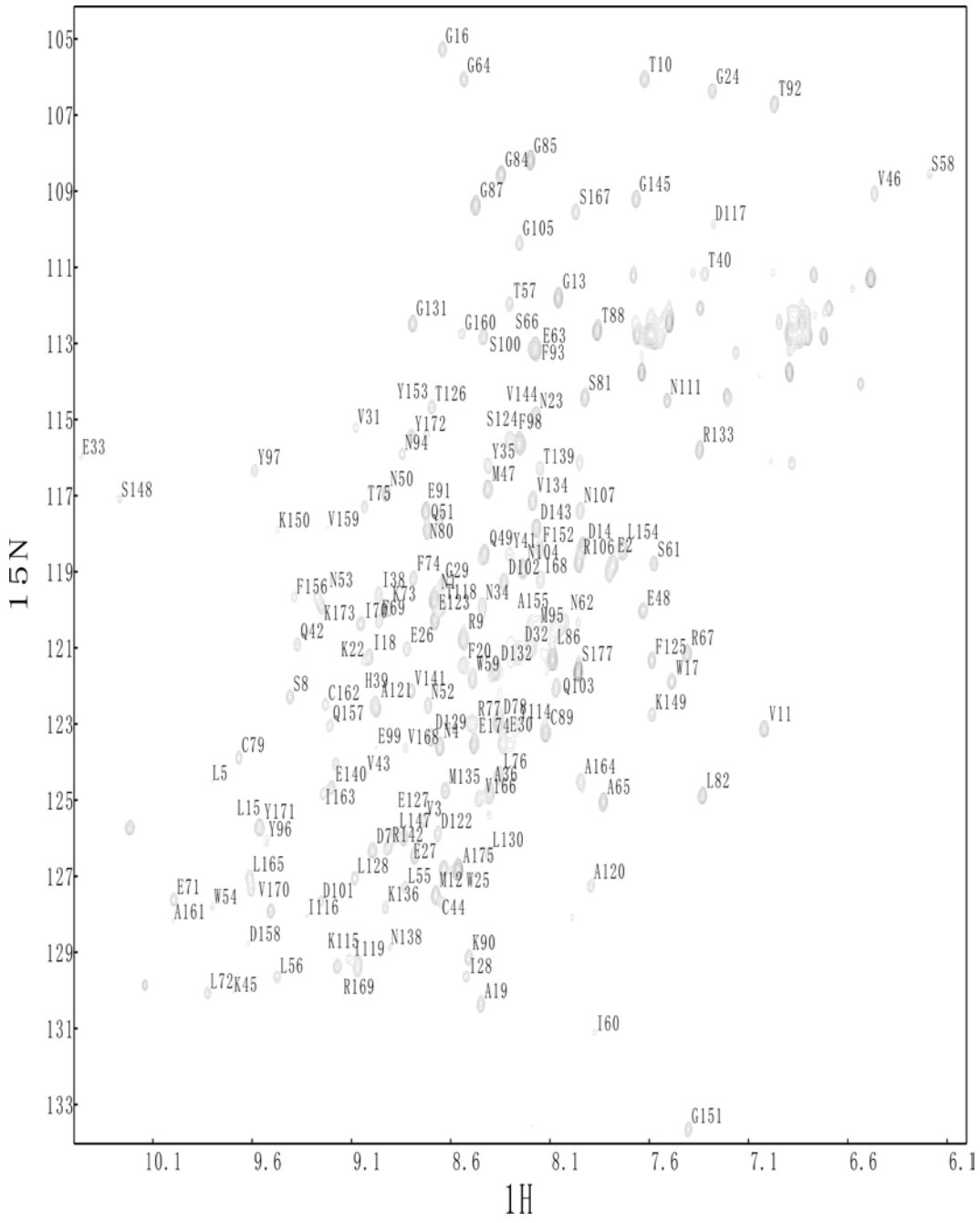

Figure 21: Assigned ^{1}H-^{15}N HSQC spectrum of the EphA5 ligand-binding domain in the presence of 3-fold WDC.

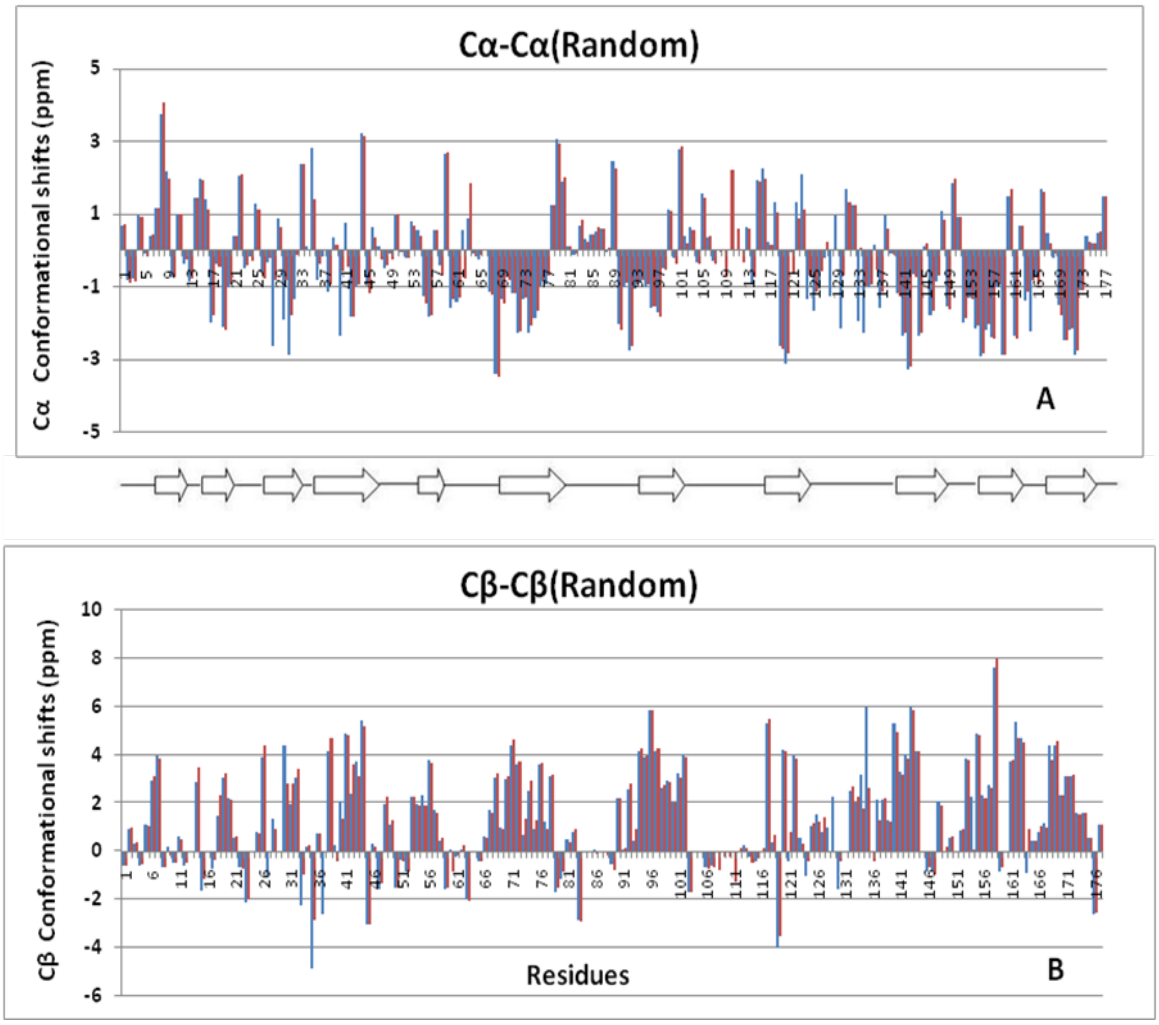

Figure 22: Secondary structures of EphA5 as calculated by ΔCα and ΔCβ. (A) Cα conformational shifts of EphA5 to Random Cα (ΔCα) in the presence (blue) and absence (red) of WDC. (B) Cβ conformational shifts of EphA5 to Random Cβ (ΔCβ) in the presence (blue) and absence (red) of WDC.

3.10.2.2 Mapping of EphA5-binding interface to WDC by chemical shift perturbation analysis

Because the chemical shift value of an NMR active atom is sensitive to its chemical environment, chemical shift perturbation analysis upon titration of ligands represents a powerful method for identifying residues that directly contact the ligands or that are indirectly affected by the binding event (Qin *et al.* 2008).

As shown in Figure 9, the HSQC peak set from the free ^{15}N-labeled EphA5 all shifted to become identical with the set from the complexes of EphA5 and WDC when the molar ratio of EphA5 to WDC reached 1:3. After further addition of WDC to a molar ratio of 1:4, the HSQC peaks did not exhibit significant further shift, indicating that the binding of EphA5 by WDC had become saturated. Therefore, to identify the interaction surfaces of EphA5 to WDC, the chemical shift differences (CSD) between the free state and the complex state (EphA5/WDC molar ratio of 1:3) were calculated according to the formula $((\Delta^1H)^2 + (\Delta^{15}N)^2/5)^{1/2}$, and the results were plotted against EphA5 sequence as shown in Figure 23.

There were twelve resonance peaks with significant CSD (residues of EphA5 with CSD larger than 1.0 ppm). Residues of I28, G29, and V31 were located on the D β-strand, E33 was located in the D-E loop, T40 was located in the E β-strand, T75 was located in the G β-strand, D122, E127, R133, and K136 were located in the J-K loop, N138 was located in the K β-strand and A164 was located in the M β-strand.

Previous data showed that D-E and J-K loops are the key components of the high affinity ephrin binding channel of the Eph receptors (Himanen *et al.* 2009; Qin *et al.*

2008). Therefore, the NMR titration results suggested that WDC probably bound to the D-E and J-K loops of the high affinity ephrin binding channel of EphA5.

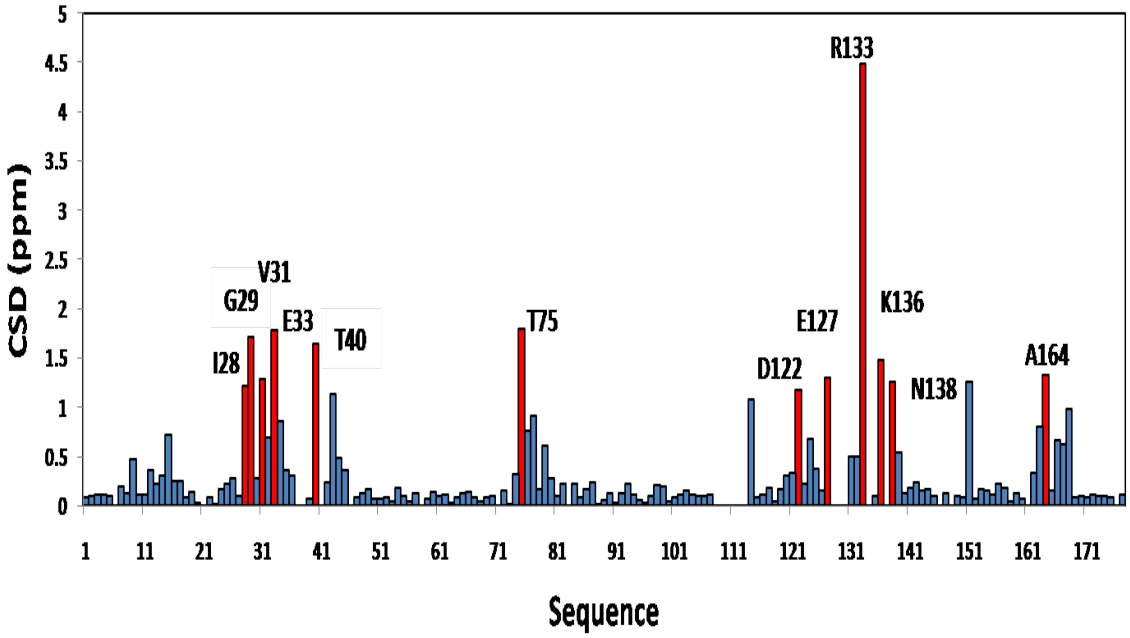

Figure 23: Residue-specific CSD of the EphA5 ligand-binding domain in the presence of 3-fold WDC. Red bars indicate residues of EphA5 with CSD larger than 1.0 ppm.

Chapter IV CONCLUSION AND FUTURE WORK

The crystal of the EphA5 ligand-binding domain was obtained. Its crystal structure showed a high degree of similarity to the previously determined ligand-binding domains of the Eph A and B receptors. EphA5 adopts the conserved jellyroll folding architecture and a compact β-sandwich.

The CD and NMR data showed that free WDC existed in a well-folded structure consisted of β-turns in solution. Residues Gly^{6} and Pro^{7} presented in the 4-residue ring formed by Cys^{5}-Cys^{10} contributed to the formation of turn structure in the peptide.

In conclusion, EphA5 and WDC possessed medium binding activity according to the NMR and ITC data. The residues of WDC involved in the interaction with EphA5 were mapped by NMR titration and Ala site-directed mutagenesis methods. Moreover, the binding surface of EphA5 to WDC was determined by chemical shift perturbation analysis from NMR titration data.

Taken all together, our results may provide critical rationales for further design of specific EphA5 antagonists for various therapeutic applications. To better understand the binding interface between EphA5 and WDC, it will be necessary to co-crystalize the EphA5 ligand-binding domain with WDC.

Chapter V REFERENCES

Battaglia AA, Sehayek K, Grist J, McMahon SB, and Gavazzi I. EphB receptors and ephrin-B ligands regulate spinal sensory connectivity and modulate pain processing (2003) *Nat. Neurosci.* 6, 339–340.

Brantley-Sieders DM, and Chen J. Eph receptor tyrosine kinases in angiogenesis: from development to disease. (2004) *Angiogenesis* 7, 17-28.

Brownlee H, Gao PP, Frisen J, Dreyfus C, Zhou R, and Black IB. Multiple ephrins regulate hippocampal neurite outgrowth. (2000) *J. Comp. Neurol.* 425, 315–322.

Caligiuri M, Molz L, Liu Q, Kaplan F, Xu JP, Majeti JZ, Ramos- Kelsey R, Murthi K, Lievens S, Tavernier J, and Kley N. MASPIT: three-hybrid trap for quantitative proteome fingerprinting of small molecule-protein interactions in mammalian cells. (2006) *Chem. Biol.* 13, 711–722.

Castellani V, Yue Y, Gao PP, Zhou R, and Bolz J. Dual action of a ligand for Eph receptor tyrosine kinases on specific populations of axons during the development of cortical circuits. (1998) *J. Neurosci.* 18, 4663–4672.

Chrencik JE, Brooun A, Kraus ML, Recht MI, Kolatkar AR, Han GW, Seifert JM, Widmer H, Auer M, and Kuhn P. Structural and biophysical characterization of the EphB4/ephrinB2 protein-protein interaction and receptor specificity. (2006) *J. Biol. Chem.* 281, 28185–28192.

Chrencik JE, Brooun A, Recht MI, Nicola G, Davis LK, Abagyan R, Widmer H, Pasquale EB, and Kuhn P. Three-dimensional structure of the EphB2 receptor in complex with an antagonistic peptide reveals a novel mode of inhibition. (2007) *J. Biol. Chem.* 282, 36505–36513.

Chrencik JE, Brooun A, Recht MI, Kraus ML, Koolpe M, Kolatkar AR, Bruce RH, Martiny-Baron G, Widmer H, Pasquale EB, and Kuhn P. Structure and thermodynamic characterization of the EphB4/Ephrin-B2 antagonist peptide complex reveals the determinants for receptor specificity. (2006) *Structure* (*Lond.*) 14, 321–330.

Emsley P, and Cowtan K. Coot: model-building tools for molecular graphics. (2004) *Acta Crystallogr. Sect. D Biol. Crystallogr.* 60, 2126–2132.

Eph Nomenclature Committee. Unified nomenclature for Eph family receptors and their ligands, the ephrins. (1997) *Cell* 90, 403–404.

Fabes J, Anderson P, Brennan C, and Bolsover S. Regeneration-enhancing effects of EphA4 blocking peptide following corticospinal tract injury in adult rat spinal cord. (2007) *Eur. J. Neurosci.* 26, 2496–2505.

Fabes J, Anderson P, Yanez-Munoz RJ, Thrasher A, Brennan C, and Bolsover S. Accumulation of the inhibitory receptor EphA4 may prevent regeneration of corticospinal tract axons following lesion. (2006) *Eur. J. Neurosci.* 23, 1721–1730.

Flanagan JG, and Vanderhaeghen P. The ephrins and Eph receptors in neural development. (1998) *Annu Rev Neurosci* 21, 309-345.

Fry DC, and Vassilev LT. Targeting protein-protein interactions for cancer therapy. (2005) *J. Mol. Med.* 83, 955–963.

Gale NW, Holland SJ, Valenzuela DM, Flenniken A, Pan L, Ryan TE, Henkemeyer M, Strebhardt K, Hirai H, Wilkinson DG, Pawson T, Davis S, and Yancopoulos GD. Eph receptors and ligands comprise two major specificity subclasses and are reciprocally compartmentalized during embryogenesis. (1996) *Neuron* 17, 9–19.

Gerlai R, Shinsky N, Shih A, Williams P, Winer J, Armanini M, Cairns B, Winslow, J, Gao W, and Phillips HS. Regulation of learning by EphA receptors: a protein targeting study. (1999) *J. Neurosci.* 19, 9538–9549.

Goldshmit Y, Galea MP, Wise G, Bartlett PF, and Turnley AM. Axonal regeneration and lack of astrocytic gliosis in EphA4-deficient mice. (2004) *J. Neurosci.* 24, 10064–10073.

Hauptman H. "Phasing methods for protein crystallography". (1997) *Curr. Opin. Struct. Biol.* **7**, 672-680.

Hu Z, Yue X, Shi G, Yue Y, Crockett DP, Blair-Flynn J, Reuhl K, Tessarollo L, and Zhou R. Corpus callosum deficiency in transgenic mice expressing a truncated ephrin-A receptor. (2003) *J Neurosci* 23, 10963–10970.

Himanen JP, Chumley MJ, Lackmann M, Li C, Barton WA, Jeffrey PD, Vearing C, Geleick D, Feldheim DA, Boyd AW, Henkemeyer M, and Nikolov DB. Repelling class discrimination: ephrin-A5 binds to and activates EphB2 receptor signaling. (2004) *Nat. Neurosci.* 7, 501–509.

Himanen JP, Goldgur Y, Miao H, Myshkin E, Guo H, Buck M, Nguyen M, Rajashankar KR, Wang B, and Nikolov DB. Ligand recognition by A-class Eph receptors: crystal structures of the EphA2 ligand-binding domain and the EphA2/ephrin-A1 complex. (2009) *EMBO Rep.* 10, 722-728.

Himanen JP, and Nikolov DB. Eph signaling: a structural view. (2003) *Trends Neurosci* 26, 46-51.

Himanen JP, Rajashankar KR, Lackmann M, Cowan CA, Henkemeyer M, and Nikolov

DB. Crystal structure of an Eph receptor-ephrin complex. (2001) *Nature.* 414, 933-938.

Himanen JP, Saha N, and Nikolov DB. Cell–cell signaling via Eph receptors and ephrins. (2007) *Current Opinion in Cell Biology* 19, 534-542. Review.

Holland SJ, Gale NW, Mbamalu G, Yancopoulos GD, Henkemeyer M, and Pawson T. Bidirectional signalling through the EPH-family receptor Nuk and its transmembrane ligands. (1996) *Nature* 383, 722-725.

Ireton RC, and Chen J. EphA2 receptor tyrosine kinase as a promising target for cancer therapeutics. (2005) *Curr. Cancer Drug Targets* 5, 149–157.

Karaman MW, Herrgard S, Treiber DK, Gallant P, Atteridge CE,Campbell BT, Chan KW, Ciceri P, Davis MI, Edeen PT, Faraoni R, Floyd M, Hunt JP, Lockhart D J, Milanov ZV, Morrison MJ, Pallares G, Patel HK, Pritchard S, Wodicka LM, and Zarrinkar PP. A quantitative analysis of kinase inhibitor selectivity. (2008) *Nat. Biotechnol.* 26, 127–132.

Kendrew JC, Bodo G, Dintzis HM, Parrish RG, Wyckoff H, and Phillips DC. A three-dimensional model of the myoglobin molecule obtained by x-ray analysis. Nature. (*1958)* 181, 662-666.

Klein R. Eph/ephrin signaling in morphogenesis, neural development and plasticity. (2004) *Curr. Opin. Cell Biol.* 16, 580–589.

Koolpe M, Burgess R, Dail M, and Pasquale EB. EphB receptor-binding peptides identified by phage display enable design of an antagonist with ephrin-like affinity. (2005) *J. Biol. Chem.*280, 17301–17311.

Koolpe M, Dail M, and Pasquale EB. An ephrin mimetic peptide that selectively targets the EphA2 receptor. (2002) *J Biol Chem* 277, 46974–46979 Kullander K, and Klein R. Mechanism and function of Eph and ephrin signaling. (2002) *Nat Rev Mol Cell Biol* 3, 475-486.

Liu J, Li M, Ran X, Fan JS, and Song J. Structural insight into the binding diversity between the human Nck2 SH3 domains and proline-rich proteins. (2006) *Biochemistry 45,* 7171–7184.

Nagpal S, Gupta V, Kaur KJ, and Salunke DM. Structure-function analysis of tritrypticin, an antibacterial peptide of innate immune origin. (1999) *J. Biol. Chem.* 24, 23296-23304.

Noberini R, Koolpe M, Peddibhotla S, Dahl R, Su Y, Cosford ND, Roth GP, and Pasquale EB. Small molecules can selectively inhibit ephrin binding to the EphA4 and EphA2 receptors. (2008) *J Biol Chem.* 283, 29461-72.

Noren NK, and Pasquale EB. Paradoxes of the EphB4 receptor in cancer. (2007) *Cancer Res.* 67, 3994–3997.

Pace CN, Vajdos F, Fee L, Grimsley G, and Gray, T. How to measure and predict the molar absorption coefficient of a protein. (1995) *Protein Sci.* 4, 2411–2423.

Pasquale, E. B. Eph receptor signaling casts a wide net on cell behaviour. (2005) *Nat Rev Mol Cell Biol.* 6, 462-75. Review.

Pasquale, EB, Eph-ephrin bidirectional signaling in physiology and disease. (2008) *Cell*. 133, 38-52. Review.

Qin H, Pu HX, Li M, Ahmed S, and Song J. Identification and structural mechanism for a novel interaction between a ubiquitin ligase WWP1 and Nogo-A, a key inhibitor for central nervous system regeneration. (2008) *Biochemistry.* 47, 13647-13658.

Qin H, Shi J, Noberini R, Pasquale EB, and Song J. Crystal structure and NMR binding reveal that two small molecule antagonists target the high affinity ephrin-binding channel of the EphA4 receptor. (2008) *J Biol Chem*. 283, 29473-29484.

Ran X, and Song J. Structural Insight into the Binding Diversity between the Tyr-phosphorylated Human EphrinBs and Nck2 SH2 Domain. (2005) *J Biol Chem.* 280, 19205-19212.

Sattler, M. Introduction to biomolecular NMR spectroscopy. (2004) (http://www.emblheidelberg.de/nmr/sattler/teaching/teaching_pdf/predoc_intro.pdf).

Shi J, Sivaraman J, and Song J. Mechanism for controlling the dimer-monomer switch and coupling dimerization to catalysis of the severe acute respiratory syndrome coronavirus 3C-like protease. (2008) *J. Virol.* 82, 4620–4629.

Tang FY, Chiang EP, and Shih CJ. Green tea catechin inhibits ephrin-A1-mediated cell migration and angiogenesis of human umbilical vein endothelial cells. (2007) *J. Nutr. Biochem.* 18, 391–399.

Wei Z, and Song J. Molecular mechanism underlying the thermal stability and pH-induced unfolding of CHABII. (2005) *J Mol Biol.* 348, 205-218.

Wilkinson DG. Multiple roles of EPH receptors and ephrins in neural development. (2001) *Nat. Rev., Neurosci.* 2, 155–164.

Wimmer-Kleikamp SH, and Lackmann M. Eph-modulated cell morphology, adhesion and motility in carcinogenesis. (2005) *IUBMB Life* 57,421–431.

Wishart DS, Sykes BD, and Richards FM. Relationship between nuclear magnetic resonance chemical shift and protein secondary structure. (1991) *J. Mol. Biol.* 222, 1-33.

Wüthrich, K. NMR of proteins and Nucleic Acids. (1986) Wiley, New York.

Yamaguchi Y, and Pasquale EB. Eph receptors in the adult brain. (2004) *Curr. Opin. Neurobiol.* 14,288–296.

Yue Y, Chen ZY, Gale NW, Blair-Flynn J, Hu TJ, Yue X, Cooper M, Crockett DP, Yancopoulos GD, Tessarollo L, and Zhou, R. Mistargeting hippocampal axons by expression of a truncated Eph receptor. (2002) *Proc. Natl. Acad. Sci. U. S. A.* 99, 10777–10782.

Appendix

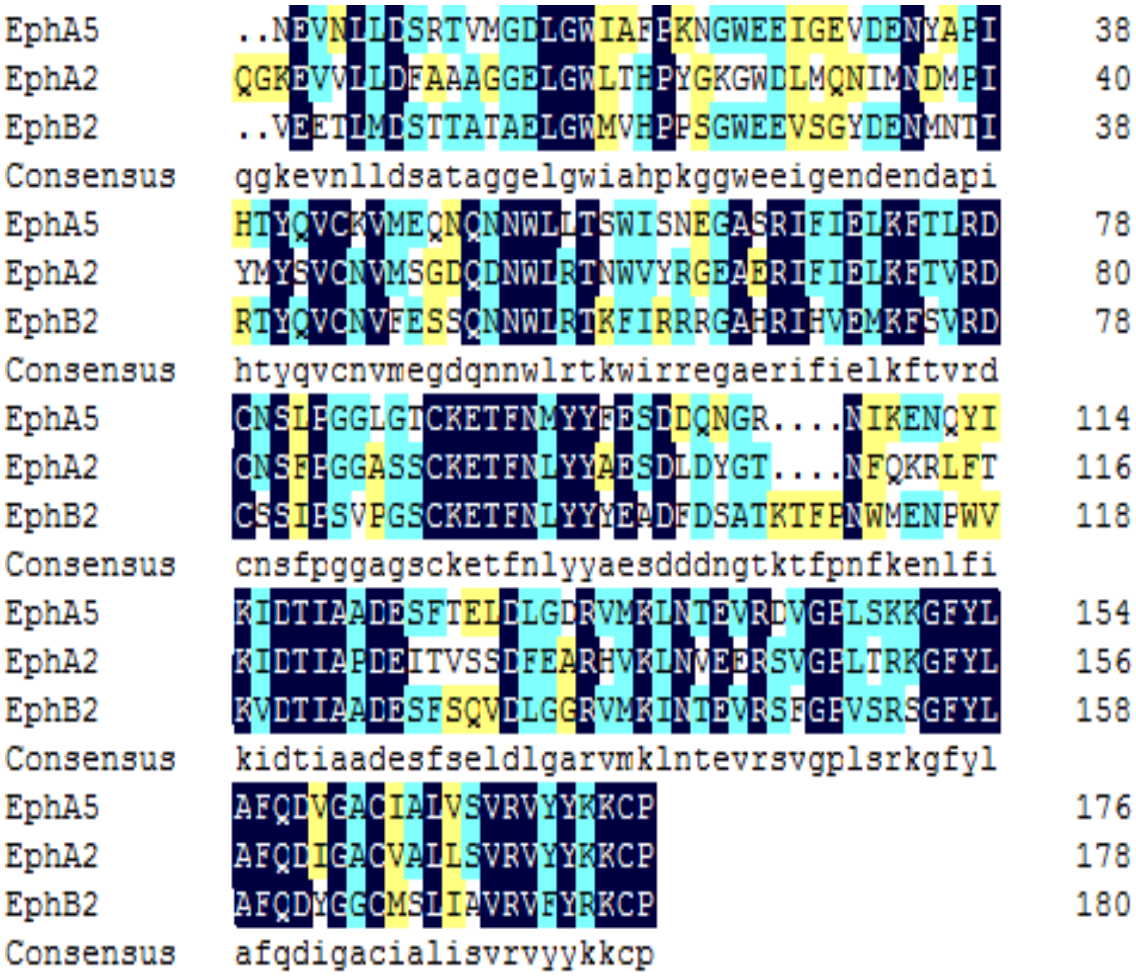

Figure 1: Sequence alignment of the ligand-binding domains of EphA5 with EphA2 and EphB2. The identical residues are colored in blue, and the homological residues are colored in light blue.

Table 1: ^{15}N, ^{15}NH and ^{13}C chemical shift of EphA5 at pH 6.3 and 25°C

NO	Residue	N	NH	Cα	Cβ
1	Asn	119.959	8.684	54.022	38.528
2	Glu	119.037	7.792	55.181	30.884
3	Val	125.764	8.744	61.734	32.18
4	Asn	123.852	8.659	54.226	38.596
5	Leu	124.696	9.798	55.307	43.571
6	Leu			55.945	45.632
7	Asp	126.748	8.943	54.158	42.145
8	Ser	122.478	9.326	62.758	63.441
9	Arg	119.735	8.566	58.458	30.747
10	Thr	106.23	7.696	61.256	69.515
11	Val	123.374	7.059	63.577	32.317
12	Met	128.295	8.711	55.523	32.454
13	Gly	111.328	8.076	44.603	
14	Asp	118.997	8.045	54.431	41.804
15	Leu	125.55	8.847	57.434	41.394
16	Gly	105.746	8.522	46.513	
17	Trp	122.331	7.629	55.796	29.45
18	Ile	121.103	9.058	61.12	41.258
19	Ala	130.088	8.423	50.609	22.556
20	Phe	121.469	8.553	54.636	41.258
21	Pro			63.372	35.457
22	Lys	121.558	9.029	58.799	32.522
23	Asn	114.928	8.166	52.861	37.095
24	Gly	106.72	7.333	45.08	
25	Trp	127.291	8.602	58.731	30.542
26	Glu	120.771	9.074	55.318	34.296
27	Glu	126.269	8.806	55.864	29.86
28	Ile	126.941	8.393	60.779	39.824
29	Gly	115.494	8.651	46.036	
30	Glu	123	8.187	55.25	32.726
31	Val	117.525	8.321	60.799	34.638
32	Asp	122.638	8.449	52.861	41.736
33	Glu	118.368	9.044	58.458	28.972

34	Asn	118.022	8.315	53.339	39.347
35	Tyr	116.323	8.061	59.686	36.07
36	Ala	125.463	8.306	50.131	18.871
37	Pro				
38	Ile			60.642	43.578
39	His	122.512	9.031	55.523	28.7
40	Thr	114.762	7.696	61.393	71.358
41	Tyr			57.843	43.715
42	Gln	120.557	9.532	54.363	33.136
43	Val	122.249	8.359	61.666	34.911
44	Cys	128.779	8.652	58.731	46.377
45	Lys	130.822	9.813	55.523	30.201
46	Val			62.963	31.975
47	Met	116.992	8.384	55.523	31.566
48	Glu	120.231	7.551	55.659	32.18
49	Gln	118.896	8.469	55.933	30.815
50	Asn	117.079	8.945	54.294	37.573
51	Gln	118.06	8.721	56.137	29.109
52	Asn	122.683	8.7	53.066	38.255
53	Asn	119.685	9.28	53.953	41.395
54	Trp	128.191	9.852	57.98	31.703
55	Leu	127.494	8.831	54.021	44.398
56	Leu	129.631	9.434	53.68	46.172
57	Thr	111.731	8.265	62.553	71.631
58	Ser			57.98	64.669
59	Trp	121.983	8.498	60.3	28.29
60	Ile	131.381	7.917	60.232	38.074
61	Ser	118.983	7.601	57.366	63.918
62	Asn	120.551	8.026	52.52	39.347
63	Glu	113.337	8.19	57.956	27.881
64	Gly	106.238	8.54	45.217	
65	Ala	125.313	7.836	52.657	18.871
66	Ser	113.332	8.19	58.731	64.669
67	Arg	121.327	7.404	55.25	32.521
68	Ile	119.288	8.143	58.116	42.145
69	Phe	120.461	8.962	56.615	40.712
70	Ile	120.577	9.053	60.779	42.009

71	Glu			54.908	34.569
72	Leu	130.41	9.806	53.27	46.241
73	Lys	119.966	8.896	55.387	34.569
74	Phe	119.865	8.805	56	42.76
75	Thr	113.411	9.487	60.301	71.289
76	Leu	125.483	8.918	54.635	46.172
77	Arg	124.776	8.046	55.796	31.839
78	Asp	122.631	8.365	54.226	41.462
79	Cys	125.218	9.63	58.526	39.688
80	Asn	117.978	8.781	55.318	38.255
81	Ser	114.223	7.941	58.799	64.464
82	Leu	125.373	7.375	52.998	42.623
83	Pro			63.85	31.907
84	Gly	109.036	8.387	45.626	
85	Gly	108.364	8.198	45.831	
86	Leu	121.691	8.087	56.137	42.419
87	Gly	109.879	8.524	45.968	
88	Thr	112.663	7.849	62.076	69.856
89	Cys	123.352	8.116	57.843	40.439
90	Lys	129.386	8.552	54.499	35.388
91	Glu	117.616	8.64	55.181	30.065
92	Thr	106.977	6.997	59.345	72.791
93	Phe	113.535	8.306	57.161	40.712
94	Asn	115.741	8.762	52.452	43.374
95	Met	120.549	8.026	54.84	36.89
96	Tyr	126.059	9.507	56.752	44.739
97	Tyr	116.529	9.587	56.478	43.169
98	Phe	115.989	8.336	57.57	42.555
99	Glu	124.01	8.946	57.161	32.795
100	Ser	112.9	8.421	58.321	66.102
101	Asp	127.842	9.261	55.864	41.394
102	Asp	119.518	8.364	53.202	42.213
103	Gln	122.379	8.084	56.751	27.812
104	Asn	119.175	8.264	52.929	39.074
105	Gly	110.537	8.207	46.855	
106	Arg	118.971	7.945	56.888	30.201
107	Asn	117.617	7.915	52.929	38.459

108	Ile	121.361	7.266	61.529	38.119
109	Lys	125.514	7.939	55.933	32.999
110	Glu	119.531	8.068	58.321	29.655
111	Asn	114.515	7.525	53.885	37.846
112	Gln	118.619	7.768	55.864	29.655
113	Tyr			58.867	39.074
114	Ile	124.255	9.194	60.847	38.46
115	Lys	129.527	9.055	58.594	32.931
116	Ile	128.282	9.329	63.577	39.074
117	Asp	110.272	7.268	53.134	43.783
118	Thr	119.955	8.684	63.031	70.675
119	Ile	129.527	9.055	58.868	35.388
120	Ala	127.812	8.047	49.926	23.444
121	Ala	121.94	8.83	52.178	20.099
122	Asp	123.345	8.398	53.885	42.146
123	Glu	119.976	8.51	57.229	30.201
124	Ser	117.002	8.236	57.98	63.713
125	Phe	121.333	7.958	56.956	40.985
126	Thr	114.572	8.557	61.393	71.221
127	Glu	123.159	8.586	56.342	31.293
128	Leu				
129	Asp				
130	Leu			54.772	42.077
131	Gly	111.413	8.679	46.718	
132	Asp	120.53	8.284	54.226	40.985
133	Arg	125.568	8.376	56.547	33.204
134	Val			61.597	33.613
135	Met	124.85	8.71	54.841	35.525
136	Lys	124.719	8.429	56.137	32.794
137	Leu	125.761	8.744	54.363	43.784
138	Asn	126.109	8.714	53.885	41.326
139	Thr	117.153	8.522	61.87	71.221
140	Glu	124.849	9.111	54.841	34.842
141	Val	122.512	8.823	60.3	34.978
142	Arg	126.748	8.943	53.271	34.774
143	Asp	118.17	8.18	52.247	44.193
144	Val	116.007	8.257	60.301	35.934

145	Gly	109.427	7.672	44.671	
146	Pro			61.324	34.16
147	Leu	126.194	8.888	54.772	41.559
148	Ser			59.55	66.034
149	Lys	122.962	7.58	55.045	33.409
150	Lys	118.053	9.463	58.662	33.818
151	Gly	130.857	7.411	46.309	
152	Phe	118.571	8.142	56.206	40.712
153	Tyr	115.676	8.807	56.956	42.691
154	Leu	118.685	7.806	53.407	42.555
155	Ala	121.205	8.181	49.926	24.126
156	Phe	120.124	9.327	56.069	42.009
157	Gln	123.43	9.184	53.749	32.112
158	Asp	128.803	9.583	52.042	46.309
159	Val	118.004	9.297	59.687	31.157
160	Gly	112.861	8.495	47.078	
161	Ala			50.336	23.103
162	Cys	121.769	9.177	56.274	45.899
163	Ile	126.513	8.966	60.437	43.442
164	Ala	127.228	8.498	51.974	20.236
165	Leu	127.047	9.757	54.568	42.965
166	Val	126.465	8.483	64.191	32.863
167	Ser	110.922	8.052	58.867	65.079
168	Val	125.797	8.794	62.485	35.593
169	Arg	129.242	9.121	54.704	35.457
170	Val	127.525	9.6	60.096	34.16
171	Tyr	125.906	9.557	56.137	42.009
172	Tyr	115.677	8.807	55.523	42.077
173	Lys	120.114	9.245	55.591	34.774
174	Glu	123.738	8.484	56.342	31.498
175	Ala	127.05	8.566	50.677	18.666
176	Pro			63.508	32.249
177	Ser	121.865	7.961	60.164	65.215

Table 2: ^{15}N, ^{15}NH and ^{13}C chemical shift of EphA5 in the presence of 3-fold WDC at pH 6.3 and 25°C

NO	Residue	N	NH	Cα	Cβ
1	Asn	119.777	8.683	53.963	38.538
2	Glu	118.825	7.782	55.26	30.825
3	Val	125.535	8.736	61.813	32.122
4	Asn	123.61	8.655	54.236	38.538
5	Leu	124.49	9.801	55.397	43.589
6	Leu			55.874	45.432
7	Asp	126.327	8.994	54.168	42.292
8	Ser	122.301	9.41	62.427	63.451
9	Arg	120.785	8.537	58.673	31.098
10	Thr	106.059	7.624	61.266	69.525
11	Val	123.141	7.021	63.605	32.413
12	Met	127.503	8.675	55.397	32.344
13	Gly	111.811	8.058	44.544	
14	Asp	118.364	7.933	54.441	41.2
15	Leu	125.719	9.564	57.444	40.859
16	Gly	105.276	8.642	46.797	
17	Trp	121.9	7.486	55.601	29.119
18	Ile	121.252	9.013	61.198	40.381
19	Ala	130.377	8.447	50.687	22.362
20	Phe	121.458	8.537	54.578	41.336
21	Pro			63.382	35.398
22	Lys	121.374	9.037	58.741	32.532
23	Asn	114.913	8.173	52.803	36.968
24	Gly	106.373	7.282	45.227	
25	Trp	126.798	8.636	58.895	30.621
26	Glu	121.034	8.821	55.465	33.829
27	Glu	126.478	8.782	55.738	28.846
28	Ile	129.644	8.523	58.946	40.244
29	Gly	119.315	8.64	46.251	
30	Glu	123.505	8.334	54.168	34.306
31	Val	115.207	9.078	59.697	33.76
32	Asp	121.153	8.266	51.643	41.354
33	Glu	115.979	10.46	58.468	27.686
34	Asn	119.907	8.441	53.417	39.289
35	Tyr	116.222	8.413	61.13	34.033
36	Ala	124.817	8.405	49.663	18.881
37	Pro			62.836	32.19

38	Ile	119.618	8.963	60.447	43.043
39	His	122.579	8.976	55.738	29.392
40	Thr	111.174	7.319	59.628	72.1
41	Tyr	118.55	8.304	59.059	43.794
42	Gln	120.917	9.372	54.373	31.917
43	Val	124.293	9.027	61.608	35.535
44	Cys	127.703	8.644	58.809	46.66
45	Lys	130.058	9.693	55.738	30.211
46	Val	109.071	6.466	63.246	32.122
47	Met	116.832	8.414	55.892	31.321
48	Glu	120.037	7.633	55.601	31.849
49	Gln	118.555	8.43	56.079	30.638
50	Asn	116.945	8.924	54.254	37.6
51	Gln	117.911	8.718	56.147	29.187
52	Asn	122.517	8.714	53.076	38.283
53	Asn	119.618	9.271	54.1	41.366
54	Trp	127.805	9.8	58.127	31.781
55	Leu	127.289	8.829	54.236	44.817
56	Leu	129.661	9.474	53.64	46.268
57	Thr	111.978	8.303	62.563	71.709
58	Ser	108.546	6.187	58.263	64.543
59	Trp	121.837	8.49	60.243	28.232
60	Ile	131.11	7.875	59.987	38.965
61	Ser	118.79	7.575	57.257	63.878
62	Asn	120.321	8.046	53.827	39.17
63	Glu	113.306	8.174	56.967	27.891
64	Gly	106.059	8.534	45.295	
65	Ala	125.05	7.831	52.53	18.881
66	Ser	113.043	8.175	58.673	64.747
67	Arg	121.157	7.409	55.328	32.6
68	Ile	119.203	8.148	58.195	41.951
69	Phe	120.288	8.961	56.762	40.79
70	Ile	120.361	9.053	60.857	41.882
71	Glu	127.625	10	54.919	34.306
72	Leu	130.075	9.824	53.213	46.114
73	Lys	119.975	8.912	55.328	33.897
74	Phe	119.164	8.788	55.806	42.292
75	Thr	117.286	9.033	60.106	70.958
76	Leu	124.361	8.356	54.509	46.114
77	Arg	123.012	8.492	55.533	32.122
78	Asp	122.983	8.361	54.236	41.405
79	Cys	123.885	9.667	58.673	39.494

80	Asn	117.382	8.726	55.192	37.992
81	Ser	114.434	7.924	58.809	64.611
82	Leu	124.891	7.33	52.94	42.497
83	Pro			63.665	31.986
84	Gly	108.572	8.346	45.705	
85	Gly	108.199	8.2	45.841	
86	Leu	121.314	8.087	56.011	42.565
87	Gly	109.38	8.474	45.978	
88	Thr	112.683	7.862	61.949	70.003
89	Cys	123.243	8.123	58.059	40.654
90	Lys	129.133	8.509	54.646	35.398
91	Glu	117.584	8.656	55.055	30.006
92	Thr	106.715	6.969	59.219	72.6
93	Phe	113.144	8.174	57.035	40.244
94	Asn	115.908	8.844	52.394	43.248
95	Met	120.429	8.048	54.782	36.832
96	Tyr	126.079	9.525	56.711	44.767
97	Tyr	116.333	9.587	56.574	43.06
98	Phe	115.529	8.3	57.581	42.429
99	Glu	123.602	8.977	57.2	32.822
100	Ser	112.826	8.435	58.468	66.112
101	Asp	127.667	9.255	55.755	41.559
102	Asp	119.295	8.331	53.367	42.31
103	Gln	122.06	8.068	56.847	27.84
104	Asn	118.942	8.237	52.957	39.152
105	Gly	110.368	8.254	46.951	
106	Arg	118.766	7.955	56.83	30.279
107	Asn	117.397	7.947	53.008	38.538
108	Ile				
109	Lys				
110	Glu				
111	Asn				
112	Gln				
113	Tyr			58.922	39.153
114	Ile	123.044	8.263	60.652	38.66
115	Lys	129.366	9.068	58.622	32.822
116	Ile	128.038	9.325	63.86	38.948
117	Asp	109.87	7.277	53.23	43.606
118	Thr	119.912	8.645	63.314	70.412
119	Ile	129.181	9.112	58.946	34.921
120	Ala	127.235	7.891	49.663	23.522
121	Ala	122.579	8.976	52.735	18.881

122	Asp	125.899	8.665	54.305	42.292
123	Glu	120.283	8.679	58.195	30.484
124	Ser	115.519	8.313	57.325	63.059
125	Phe	121.332	7.587	56.42	40.859
126	Thr	114.675	8.695	60.925	71.573
127	Glu	125.998	8.836	55.874	30.689
128	Leu	127.051	9.082	54.236	43.521
129	Asp	123.36	8.7	53.963	40.586
130	Leu	126.418	8.407	53.349	40.927
131	Gly	112.485	8.792	47.07	
132	Asp	121.607	8.376	54.236	40.79
133	Arg	115.799	7.346	54.527	32.959
134	Val	117.15	8.187	60.328	35.006
135	Met	124.76	8.627	54.782	38.897
136	Lys	127.827	8.929	56.83	33.146
137	Leu			53.895	44.681
138	Asn	128.872	8.907	54.236	41.268
139	Thr	116.292	8.149	61.881	71.3
140	Glu	124.671	9.2	54.919	35.194
141	Val	122.132	8.799	60.243	35.125
142	Arg	126.248	8.915	53.213	34.921
143	Asp	117.852	8.169	52.325	44.271
144	Val	115.63	8.254	60.243	35.944
145	Gly	109.207	7.667	44.613	
146	Pro			61.216	33.983
147	Leu	125.931	8.883	54.646	41.678
148	Ser	117.089	10.267	59.765	66.181
149	Lys	122.761	7.585	55.124	33.146
150	Lys	117.885	9.471	58.554	33.778
151	Gly	133.662	7.403	46.319	
152	Phe	118.415	8.153	56.079	40.654
153	Tyr	115.368	8.721	56.967	42.77
154	Leu	118.403	7.734	53.349	44.749
155	Ala	120.985	8.199	49.868	24.205
156	Phe	119.666	9.387	55.874	42.156
157	Gln	123.038	9.209	53.776	32.276
158	Asp	128.759	9.619	51.984	45.909
159	Val	117.818	9.218	59.697	30.962
160	Gly	112.744	8.543	46.865	
161	Ala	128.163	9.996	50.414	23.045
162	Cys	122.484	9.231	56.284	46.592
163	Ile	124.846	9.243	60.192	43.606

164	Ala	124.538	7.945	50.551	18.403
165	Leu	127.045	9.613	54.782	42.975
166	Val	124.995	8.456	64.27	32.6
167	Ser	109.547	7.97	59.151	65.293
168	Val	123.624	8.827	62.359	36.217
169	Arg	129.38	9.173	54.987	35.33
170	Val	127.327	9.604	60.124	34.119
171	Tyr	125.719	9.564	56.097	42.036
172	Tyr	115.442	8.798	55.414	42.036
173	Lys	119.913	9.252	55.601	34.784
174	Glu	123.536	8.482	56.489	31.508
175	Ala	126.867	8.563	50.687	18.676
176	Pro			63.468	32.208
177	Ser	121.631	7.957	60.174	65.225